

# Human Photoreceptor Topography

CHRISTINE A. CURCIO, KENNETH R. SLOAN, ROBERT E. KALINA,  
AND ANITA E. HENDRICKSON

Departments of Biological Structure (C.A.C., A.E.H.), Ophthalmology (C.A.C., R.E.K., A.E.H.), and Computer Science (K.R.S.), University of Washington, Seattle, Washington 98195

## ABSTRACT

We have measured the spatial density of cones and rods in eight whole-mounted human retinas, obtained from seven individuals between 27 and 44 years of age, and constructed maps of photoreceptor density and between-individual variability. The average human retina contains 4.6 million cones (4.08–5.29 million). Peak foveal cone density averages 199,000 cones/mm<sup>2</sup> and is highly variable between individuals (100,000–324,000 cones/mm<sup>2</sup>). The point of highest density may be found in an area as large as 0.032 deg<sup>2</sup>. Cone density falls steeply with increasing eccentricity and is an order of magnitude lower 1 mm away from the foveal center. Superimposed on this gradient is a streak of high cone density along the horizontal meridian. At equivalent eccentricities, cone density is 40–45% higher in nasal compared to temporal retina and slightly higher in midperipheral inferior compared to superior retina. Cone density also increases slightly in far nasal retina. The average human retina contains 92 million rods (77.9–107.3 million). In the fovea, the average horizontal diameter of the rod-free zone is 0.350 mm (1.25°). Foveal rod density increases most rapidly superiorly and least rapidly nasally. The highest rod densities are located along an elliptical ring at the eccentricity of the optic disk and extending into nasal retina with the point of highest density typically in superior retina (5/6 eyes). Rod densities decrease by 15–25% where the ring crosses the horizontal meridian. Rod density declines slowly from the rod ring to the far periphery and is highest in nasal and superior retina. Individual variability in photoreceptor density differs with retinal region and is similar for both cones and rods. Variability is highest near the fovea, reaches a minimum in the midperiphery, and then increases with eccentricity to the ora serrata. The total number of foveal cones is similar for eyes with widely varying peak cone density, consistent with the idea that the variability reflects differences in the lateral migration of photoreceptors during development. Two fellow eyes had cone and rod numbers within 8% and similar but not identical photoreceptor topography.

**Key words:** retina, cones, rods, fovea

The mosaic formed by the rod and cone photoreceptors initiates the visual process by converting the continuous image transmitted by the ocular optics to a discrete array of signals. The photoreceptor mosaic thus provides all the spatial information available to higher stages of visual processing and imposes fundamental limitations on this processing. Recent theoretical and psychophysical investigations have defined anatomical parameters of the photoreceptor mosaic that determine how much information is retained or lost by sampling. These parameters include photoreceptor spacing, the geometry of the sampling array, and diameters of photoreceptor apertures (French et al., '77; Yellott, '82; Williams and Collier, '83; Miller and Barnard, '83; Hirsch and Hylton,

'84b; Ahumada and Poirson, '87). It has become clear that these anatomical properties have specific consequences for visual functions such as resolution acuity (Campbell and Green, '65; Green, '70; Snyder and Miller, '77; Miller, '79; Hirsch and Miller, '87; Williams, '85, '86; Hirsch and Curcio, '89), detection acuity (Thibos et al., '87), spatial discrimination (Hirsch and Hylton, '82, '84a; Geisler and Hamilton, '86; Groll and Hirsch, '87), and pattern recognition (Williams and Coletta, '87; Coletta and Williams, '87; Smith and Cass, '87). Furthermore, the striking regional heterogeneity

Accepted August 11, 1989.

of the primate photoreceptor mosaic (Schultze, 1866; Østerberg, '35; Curcio et al., '87b) means that this initial extraction of spatial information in the retinal image differs across the visual field. Thus efforts to determine how visual function is limited by the two-dimensional sampling properties of the human photoreceptor mosaic require accurate measures of its functionally relevant anatomical parameters across the entire retina.

Of the parameters noted above, the overall spatial density of photoreceptors ( $\text{cells/mm}^2$ ) in the human retina (and, hence, mean spacing) has been best characterized, although even these data are surprisingly sparse. The modern era of the photoreceptor mosaic began with the classic study of Østerberg ('35), who was the first to measure photoreceptor density at well defined retinal locations and to provide a topographic description. He quantified for a single retina such salient features of the cone distribution as the high density in the all-cone foveola, the rapid decrease in cone density within several degrees of the foveal center, and the higher density in the nasal compared to temporal retina. For rods, he observed a rod-free zone in the fovea with a rapid increase in density to an annulus of high rod density at approximately  $20^\circ$ , and a slow decline into the far periphery. Information that is less extensive but qualitatively consistent with Østerberg is available from Polyak ('41), who reported ratios and center-to-center spacing of rods and cones from seven retinal regions, and from Farber et al. ('85), who reported photoreceptor density in 16 retinal zones of four eyes. Our recent description of the cone distribution in four densely sampled adult retinas (Curcio et al., '87b) has confirmed the overall topography described by Østerberg as well as validated his density values for most of the peripheral horizontal meridian.

Because of the importance of the cone-rich fovea for high acuity vision, more knowledge of its detailed anatomy is especially needed. There are several estimates for the maximum density (or minimum spacing) of cones in the adult fovea (Østerberg, '35; Hartridge, '50; O'Brien, '51; Miller, '79; Farber et al., '85; Yuodelis and Hendrickson, '86; Ahnelt et al., '87), which range from  $49,600/\text{mm}^2$  (Farber et al., '85) to  $238,000/\text{mm}^2$  (Ahnelt et al., '87). These studies encompass a variety of histological techniques and a range of ages, and many of these studies are based on only one or two eyes. The limitations imposed by small sample size are particularly important, because we have recently found (Curcio et al., '87b) a threefold variability in the peak cone density of eyes from normal, adult human donors.

Several recent technical advances now make anatomical investigation of the human photoreceptor mosaic more feasible. First, well fixed human retinas obtained shortly after death are more readily available through donor programs. Second, we have developed a whole-mount method that preserves topography and morphological detail and eliminates the substantial artifacts that can be caused by histological processing and sectioning (Curcio et al., '87a). Finally, the application of microcomputer and video technology can assist in collection and analysis of morphometric data from a tissue whose large area and local uniformity make a large-scale survey a tedious and potentially error-prone task (Curcio et al., '89). Using these technical advances, we extend our previous work on the spatial distribution of cones in human retina (Curcio et al., '87b) in several ways: 1) we expand our sample to eight eyes, including a pair of fellow eyes and a surgical specimen whose visual function was documented; 2) we describe the distribution of rods; 3) we have created

maps of an average retina, which reveal features not easily seen in maps of individual eyes; and 4) we provide a more detailed analysis of between- and within-individual variability. Abstracts of this work have been reported (Curcio et al., '86a,b).

## MATERIALS AND METHODS

### Tissue collection, tissue preparation, and criteria for selection

Human retinas were obtained from eye bank donors within 3 hours of death. Donors had no history of eye disease or chronic neurologic disease. The anterior segment was removed just posterior to the corneoscleral limbus (even if the cornea was not transplanted), and the globes were fixed by immersion in 0.1 M phosphate-buffered 4% paraformaldehyde-0.5% glutaraldehyde for periods ranging from weeks to months. In all, 49 donor eyes from individuals 20–45 years of age were obtained over a period of 3.5 years, and seven eyes from six individuals aged 27–44 years (Table 1) met the criteria (see below) for use. One additional eye was obtained from a 32-year-old woman who had an exenteration of the right orbit for recurrent mucoepidermoid carcinoma of the ethmoid sinus. The right orbit had been treated with 6,500 rads of external beam radiation 2 years previously, without shielding of the eye. The patient had no visual complaints prior to surgery. Complete eye examination performed 2 months prior to surgery showed visual acuity of 20/20 in each eye with correction of low myopia. Examination was normal, with the exception of several small hemorrhages in the nerve fiber layer adjacent to the right optic disc, thought to be due to mild radiation retinal vasculitis. Goldmann visual field testing was normal in both eyes. Indirect ophthalmoscopy just prior to enucleation of the right eye showed no abnormalities. The eye was enucleated under general anesthesia and immediately injected through the pars plana with 0.2 cc of the standard fixative. The eye was placed in a large volume of the same fixative and, after 15 minutes, was opened through the pars plana of the nasal side with a blade.

Whole mounts of fixed retina were prepared for revealing photoreceptors with a combination of Nomarski differential interference contrast microscopy (NDIC) and video as previously described (Curcio et al., '87 a,b). While still in the globe, the retina was cut into a three-piece whole mount amenable to computer reconstruction of the original retinal sphere: 1) a belt approximately 12 mm wide centered on the horizontal meridian, 2) an inferior cap, and 3) a superior cap. The resulting pieces of retina were flattened on plastic slides with photoreceptors up, rinsed in water, cleared overnight under a coverslip with 100% dimethylsulfoxide (DMSO), and mounted with 100% glycerol under a fresh coverslip that was sealed around the edges with nail polish. Retinas H5L-H7 all exhibited small degrees of areal expansion during processing (Table 2), as determined by comparing outline drawings of the tissue in buffer and DMSO. Other similarly prepared specimens showed a range of 2–12% areal (0.9–5.8% linear) expansion (Curcio et al., '87a). Density and spacing estimates were not corrected for this small expansion.

The fact that we had access to many donor eyes allowed us to apply a rigorous two-stage screening protocol to ensure well preserved morphology. First, eyes were inspected under the dissecting microscope to exclude ocular disease and

TABLE 1. Subjects

Case	Eye	Age (years)	Sex	Time (min) to		Cause of death
				Enucleation	Fixation	
H1	R	44	F	23	127	Subarachnoid hemorrhage
H2	L	27	M	15	n.a.	Multiple trauma
H3	L	35	F	90	n.a.	Brain tumor
H4	L	34	M	95	120	Head injury and respiratory arrest
H5	L, R	35	F	27	115	Head injury
H6	L	36	M	111	146	Pulmonary embolism
H7	R	32	F	—	15 <sup>1</sup>	Mucoepidermoid carcinoma of ethmoid sinus <sup>1</sup>

<sup>1</sup>Surgical enucleation; see text for details.

TABLE 2. Morphometric Methods

Eye	Size of sampling window <sup>1</sup>	Adjacent windows in foveola	Sampling pattern <sup>2</sup>	Stage control <sup>3</sup>	Sample size		Tissue and model area			
					Cones		Rods			
					Extent mapped	Total pts	Extent mapped	Total pts		
H1	Large	9	1	Manual	Whole eye	253	Belt, I cap	195	—	0.829
H2	Large	25	2	Manual	To 5 mm ecc.	132	To 5 mm ecc.	127	—	—
H3	Large	15	2	Manual	Whole eye	163	Whole eye	155	—	0.828
H4	Large	15	3	Manual	Whole eye	192	Whole eye	169	—	0.901
H5L	Large	28	3	Manual	Whole eye	204	Whole eye	198	1.060	0.963
H5R	Small	42	3	Computer	Whole eye	213	To 6 mm ecc.	121	—	0.909
H6	Small	35	3	Computer	Whole eye	171	—	—	1.022	0.947
H7	Small	35	3	Computer	Belt	149	—	—	1.053	—

<sup>1</sup>Size of sampling window and number of windows at each data point. Large: 53 × 36.4 μm (100×); 130 × 88 μm (40×); 1 100× window for cones <1 mm from foveal center and for all rods; 1 40× window for cones peripheral to 1 mm from foveal center; 12 adjacent 100× windows at ora serrata. Small: 45.4 × 29.3 μm (100×); 108 × 74 μm (40×); 1 100× window for cones <0.25 mm from foveal center and for all rods; 2 adjacent 100× windows for all rods and cones 0.25–1 mm for foveal center; 2 adjacent 40× windows for cones peripheral to 1 mm from foveal center; 12 adjacent 100× windows at ora serrata. <sup>2</sup>Sampling patterns for retina >0.2 mm from foveal center; 1, Triangular lattice whose spacing increased with eccentricity; 2, same as pattern 1 with additional points at 2 mm intervals posterior to ora serrata; 3, points along spiral (Curcio et al., 1989) for belt, triangular lattice for caps, and at 2 mm intervals posterior to ora serrata; <sup>3</sup>Manual, accurate to 100 μm in periphery; adjacent foveal windows placed by direct observation. Computer, accurate to 1 μ. <sup>4</sup>Ratio of tissue area after DMSO clearing to tissue area in buffer. <sup>5</sup>Ratio of model area for cone distribution to area of DMSO-cleared tissue.

TABLE 3. Summary

Eye	Cones						Rods					
	Retinal area (mm <sup>2</sup> )	Fovea disk (mm) <sup>1</sup>	Peak density (cones/mm <sup>2</sup> × 1,000)	Total number (millions)	Mean density (cones/mm <sup>2</sup> × 1,000)	Central-peripheral gradient <sup>2</sup>	Peak density (rods/mm <sup>2</sup> × 1,000)	Quadrant of peak <sup>3</sup>	Eccentricity of peak (mm)	Total number (millions)	Mean density (rods/mm <sup>2</sup> × 1,000)	Rod/cone ratio
H1	1,105.3	3.70	311.0	4.72	4.26	83.16	189.0	S-T	4.2	—	—	—
H2	—	3.39	98.2 <sup>4</sup>	—	—	—	186.0	S-N	4.0	—	—	—
H3	856.1	3.53	120.0	4.08	4.76	28.05	158.0	I-T	3.8	77.87	90.96	19.09
H4	964.2	3.86	181.8	5.29	5.48	34.37	181.0	S-N	4.0	107.27	111.25	20.28
H5 <sup>5</sup>	1,104.5	3.44	178.3	4.43	4.00	52.79	167.0	—	—	—	—	—
H6	975.7	3.16	324.1	4.47	4.57	82.25	—	—	—	—	—	—
H7	1,106.0	3.55	181.1	—	—	—	—	—	—	—	—	—
Mean	1,018.6	3.58	199.2	4.60	4.62	56.12	176.2	—	4.1	91.96	94.85	20.24
SD	103.7	0.19	87.2	0.45	0.56	25.91	13.2	—	0.2	14.74	14.84	1.13
H5-L	1,101.7	3.39	186.3	4.25	3.85	51.57	161.0	S-N	3.8	90.73	82.35	21.35
H5-R	1,107.2	3.49	190.3	4.61	4.16	54.01	173.0	S-N	5.0	—	—	—
Osterberg (35)	—	—	147.3	6.23	5.3 <sup>7</sup>	—	170.0	S-N	6.2	110.0	104.1 <sup>7</sup>	17.04

<sup>1</sup>Foveal center to temporal edge of disk.<sup>2</sup>Peak density/mean density at eccentricities > 14 mm.<sup>3</sup>N, nasal; T, temporal; S, superior; I, inferior.<sup>4</sup>Not at foveal center.<sup>5</sup>H5-L and H5-R weighted as one individual throughout; see below for separate data.<sup>6</sup>See individual data for H5-L and H5-R.<sup>7</sup>In part of retina comparable to the average retina.

postmortem folds and detachment in the posterior retina. Second, cleared whole mounts of retinas without such gross artifacts were further inspected by using high-magnification NDIC-video imaging to exclude specimens with microscopic artifacts. The peripheral retina of many eyes had patches of optically indistinct photoreceptors lying oblique to the line of sight in the microscope (Curcio et al., '87a). This artifact was assumed to be a result of the postmortem retinal

detachment commonly found in donor eyes. Because areas of good morphology usually could be found nearby, such patches did not disqualify an eye from further study. However, many donor eyes were rejected because of poorly preserved foveal morphology. Frequently, cone inner segments appeared optically indistinct, which may have resulted from a slight macular detachment undetectable in the initial macroscopic inspection. There were also numerous breaks

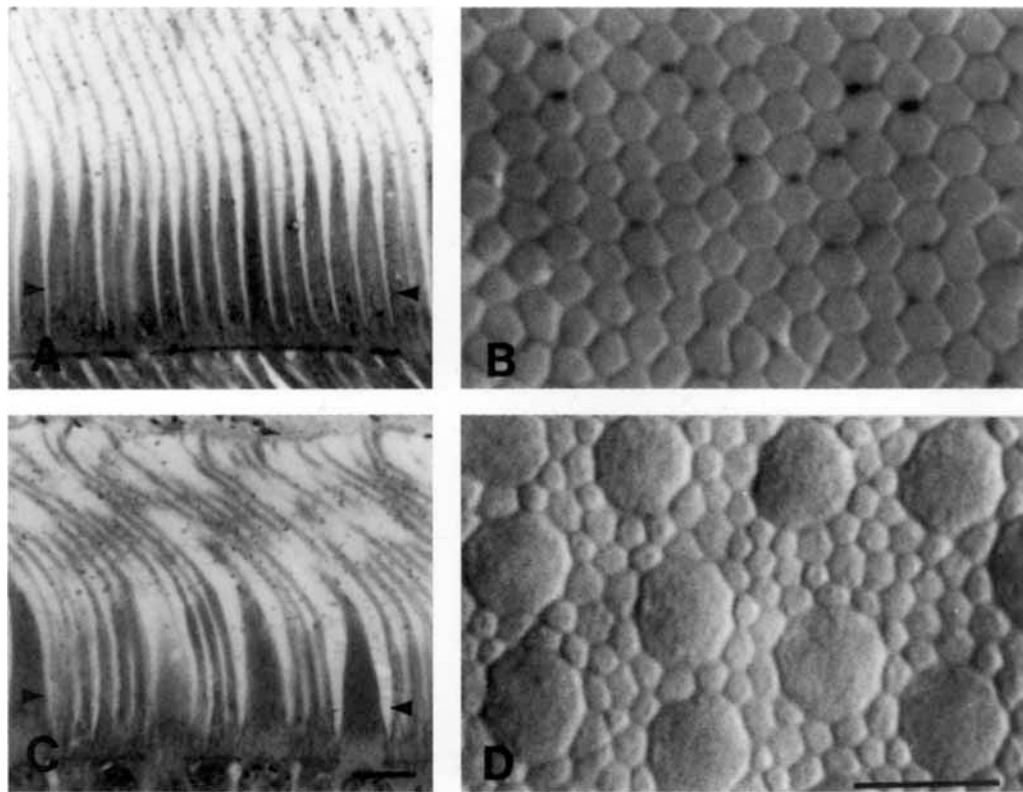


Fig. 1. Comparison of vertical histological (A,C) and en face optical (B,D) sections through photoreceptors in the fovea (A,B) and near periphery (C,D) of human retina. Arrowheads in A,C indicate approximate level through the ellipsoid portion of photoreceptor inner segments where photographs B,D are taken. The external limiting mem-

brane is the discontinuous dark line passing through the letters A and C. Tissue shown in A and C is from 2- $\mu\text{m}$ -thick glycol methacrylate sections stained with azure II methylene blue. All profiles in B are cones; large profiles in D are cones, and small intervening profiles are rods. Scale bar for histological sections = 10  $\mu\text{m}$ . Bar for optical sections = 10  $\mu\text{m}$ .

in the external limiting membrane (ELM) in the foveola. These breaks are probably attributable to differential tissue volume changes between the cone inner segments and the ELM, such that the inner segments swell relative to the inelastic ELM (Bunt-Milam et al., '85). This artifact is particularly insidious, since the packing of the inner segments still looks approximately triangular, but the density measured at the level of inner segments is 15–20% lower than the density at the level of the ELM. Finally, many eyes had such steeply sloped walls in the fovea that the photoreceptors presented an almost longitudinal rather than cross-sectional view. The retina from the surgical case had unusual cysts in the myoids of cone inner segments, particularly in the fovea, which greatly distorted the appearance of the photoreceptor mosaic at this level. However, this eye was used because the ELM was intact, and the photoreceptor mosaic at the level of the ellipsoids appeared normal. It is not clear whether this finding was attributable to postenucleation artifact or to the clinical history of radiation treatment.

### Morphometric data collection

Morphometric methods used for different eyes are summarized in Table 2. More details are available elsewhere (Curcio and Sloan, '86; Curcio et al., '89).

**Window size.** Counts were made from NDIC-video images of the photoreceptor layer at the level of inner seg-

ments, using the stylus of a graphics tablet to mark counted cells (Curcio and Sloan, '86). Throughout the retina, rods were counted by using the 100 $\times$  objective. Cones were counted at 100 $\times$  within the fovea and at 40 $\times$  when they were surrounded by a ring of rods, about 1 mm from the foveal center. The size of the video image was scaled using a calibrated slide viewed in horizontal and vertical orientations, and adjustments were made in the camera's internal size controls as necessary. Counts from adjacent windows were pooled when cell density was low (Table 2). To assess sampling variability in the peripheral retina, rods and cones were counted in six adjacent 100 $\times$  windows at ten locations along the horizontal meridian from 1 to 17 mm from the fovea in eye H4. The range of counts obtained for both photoreceptor types were compared across eccentricities and between the two video cameras used. For both rods and cones, the standard error of the mean density was 4–8% at most locations and showed no obvious trends with eccentricity or the camera used. Counts by two observers for the same windows of peripheral retina generally differed by less than 1% and infrequently differed by more than 2%.

In the foveal center, a small area of high density may be diluted by surrounding areas of lower density if it is included in a large window (Curcio et al., '87b; Hirsch and Miller, '87). All peak foveal densities are expressed for the smaller 100 $\times$  window, which was used routinely for all eyes subsequent to H5L and therefore the remeasured values for

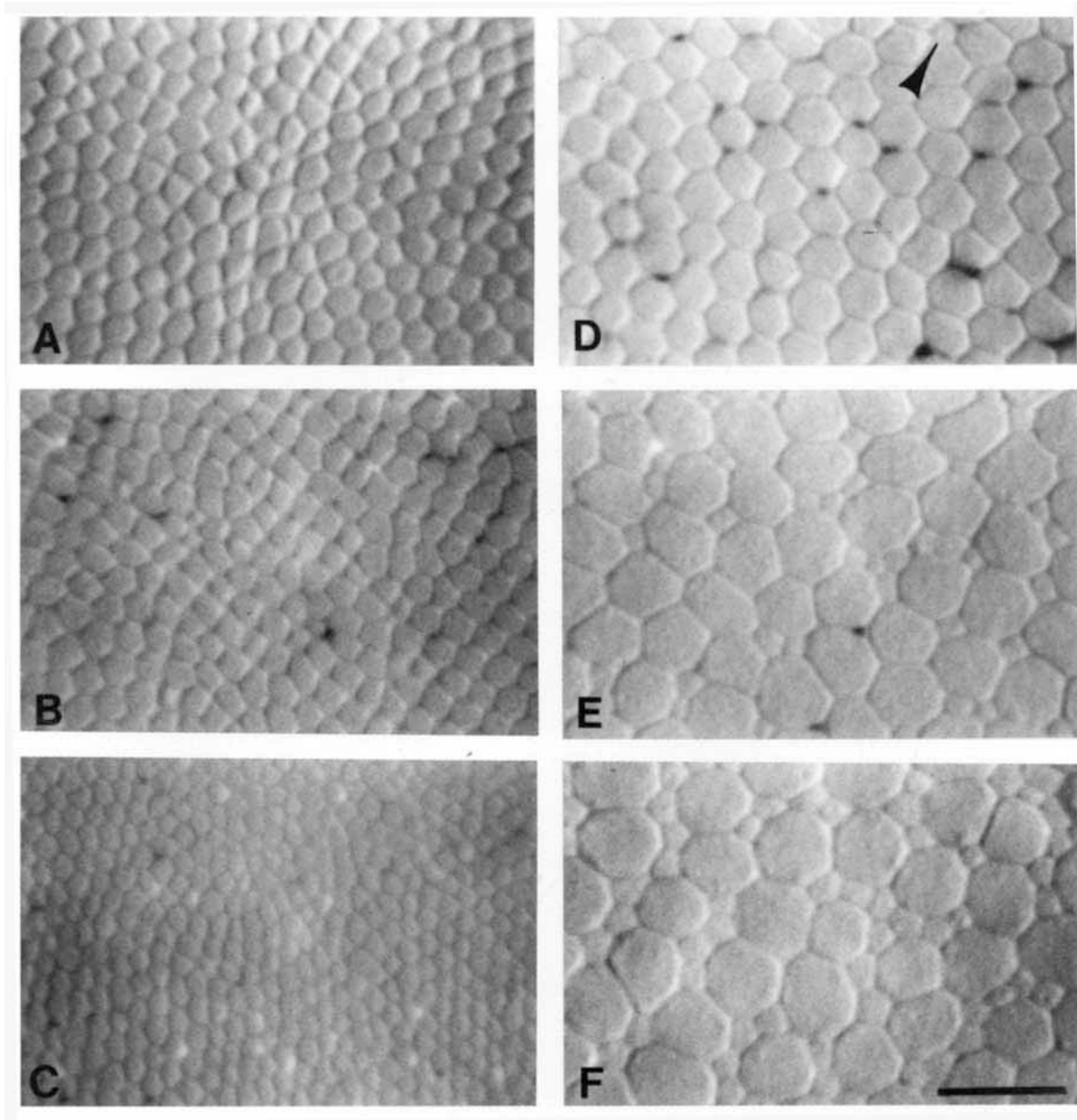


Fig. 2. Optical sections of the foveal cone mosaic, showing between-individual variability at the foveal center and variation in cell density and size with eccentricity. A-C: Foveal centers, containing only cones, of H5L (A), H4 (B), and H6 (C). Note much higher density of cones in H6. D: Edge of rod-free zone in H4, 0.125 mm temporal to the foveal center. Arrowhead points to one rod. Note that cone inner segments are

much larger than at foveal center (B). E: Point of equal rod and cone density, 0.42 mm nasal to foveal center in H4. F: Foveal slope, 0.66 mm temporal to foveal center of H5L. The small rods outnumber the large cones by about 4:1; rods form incomplete rings around cones. Bar = 10  $\mu\text{m}$ .

H1, H2, and H4 are higher than previously reported (Curcio et al., '87b). The central foveal field of H3 was not available for recounts with the smaller window, and its adjusted density was estimated by extrapolation of cone density functions along cardinal meridians.

**Location of sampling windows.** The foveal center was densely sampled with a grid of multiple adjacent windows so that the site of peak density would not be missed (Table 2). For the peripheral retina, we used two basic sampling schemes in which data points were approximately

locally equidistant and whose distance from each other increased with eccentricity. At 2 mm intervals around the anterior edges of the belt and caps, additional samples were included at the first field posterior to the ora serrata where cones and rods were reliably distinguishable. Despite generally poorer tissue preservation near the ora serrata, cones could still be counted because they were refractive and widely separated. In contrast, individual rods were not easily resolved within the overall texture of the rod mosaic; therefore, they were not counted as close to the ora serrata

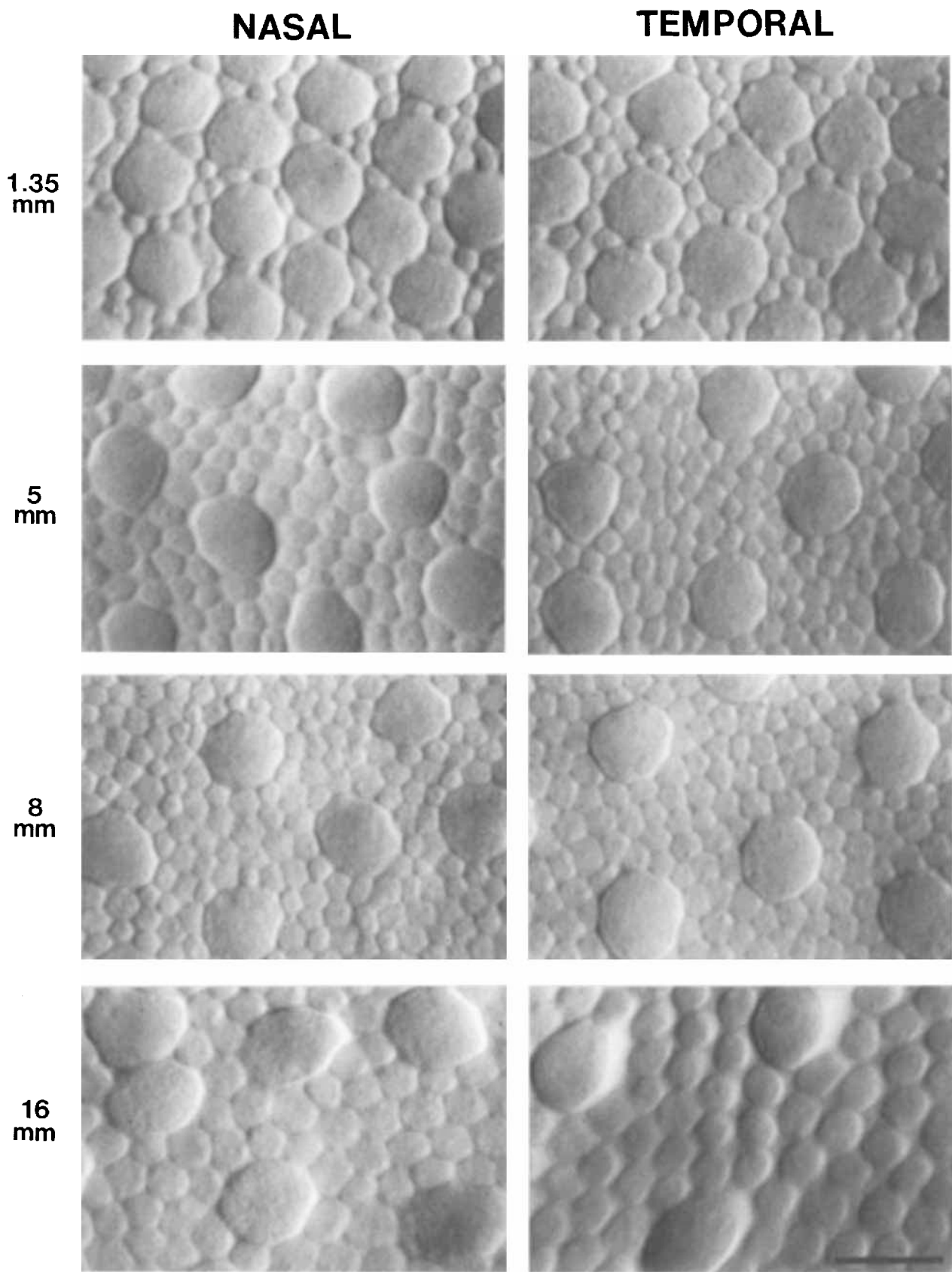


Fig. 3. Peripheral photoreceptor mosaic at corresponding eccentricities in nasal (left column) and temporal (right column) retina in H5L showing eccentricity dependent changes in photoreceptor density and inner segment diameter. Eccentricity is given along the left edge. Cones are large profiles and rods are small profiles throughout. Scale bar = 10  $\mu\text{m}$ . See text for details.

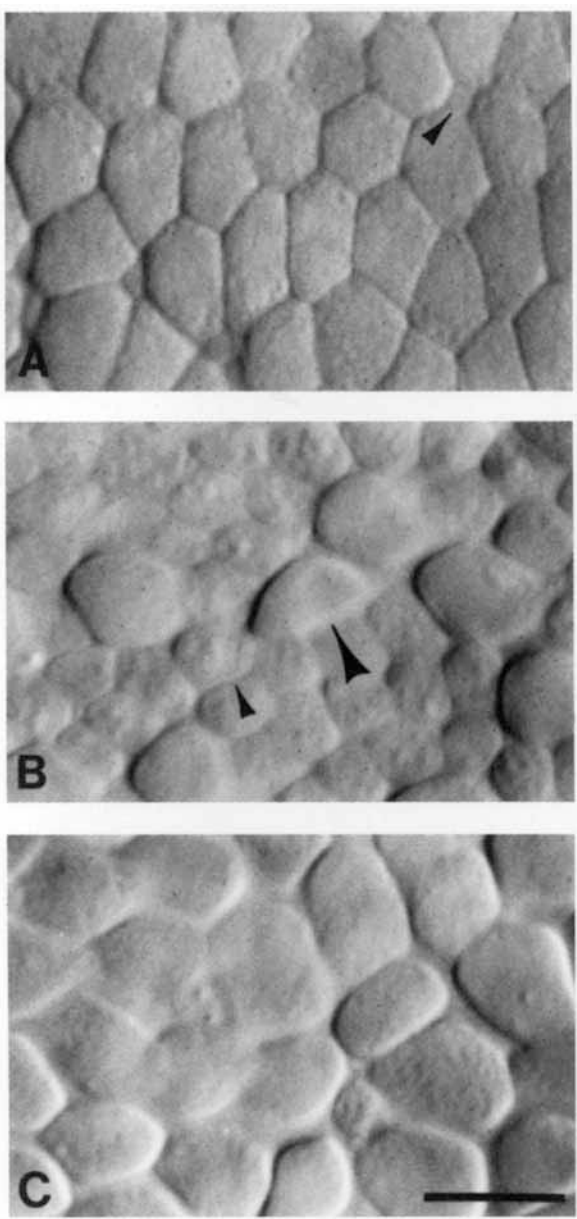


Fig. 4. Photoreceptor mosaic at sites in nasal retina which have no equivalent in temporal retina. **A:** Patch of large and irregularly polygonal cones, adjacent to optic disk in H4. There are a few intervening rods (arrowhead). **B:** Extreme nasal periphery of H6, 21 mm from foveal center. Note elliptical profiles of cone inner segments (large arrowhead) and large rods (small arrowhead). **C:** Cells of unknown identity, 22 mm from foveal center of H6. Bar = 10  $\mu\text{m}$ .

as were cones. Programs created lists of x,y coordinates of sample points to which the data collection programs directed either a manual or computer-controlled microscope stage (Table 2). Because slide position in the stage specimen holder was variable, the positions of well defined tissue landmarks were used to back-transform data points to their original locations at each data collection session.

### Reconstruction, display, and analysis

We created for each eye a digital model (Curcio et al., '89) of photoreceptor density distributions, in which data points were indexed by coordinates in a spherical coordinate system: meridian (longitude) and eccentricity (colatitude). Construction of the model required 1) estimated retinal radius and the locations in tissue x,y coordinates of 2) photoreceptor densities, 3) the foveal center (defined as the field with the highest cone density), 4) the center of the optic disk, and 5) the cut ends of blood vessels at the edges of the whole-mount pieces. Data points were connected into a mesh of triangular patches closely approximating the surface of a sphere. A weighted mean of values at the three vertices of a patch was similar to the density found in the tissue itself at that location, even in the fovea, where cell densities change rapidly. Data interpolated in this manner were used to create graphs of density or derived parameters (e.g., rod:cone ratio) along selected meridians of individual eyes. False color maps of isodensity contours were created by interpolating across triangular patches and assigning colors to small ranges of density values. Meridian plots and maps of average density (or derived parameters) were obtained by resampling each eye at a set of standard locations, which were normalized by geometric degrees of arc along the retinal sphere, with retinal directions (nasal, superior, etc.) preserved. The averaged cone data is taken from seven individuals and rod data from five individuals. Data from fellow eyes were averaged and weighted as one individual (Ederer, '73).

We calculated the total number of cells and total area in specific regions or the entire retina from the mean density of a triangular patch and its area (on the spherical surface). The total area of the model is 4–17% (Table 2) smaller than the actual area of the whole mount (Table 3), indicating reasonable preservation of spatial relationships in the reconstruction process. We corrected the total number of cells for missing tissue area by including the product of the mean density at the endpoints of the primary meridians and the areal difference between the model and the tissue. Since retinas differed in size and extent mapped, averaged data (see above) are not shown for far peripheral eccentricities where the number of specimens included was fewer than two, and the total area encompassed by the model of the average retina ( $843 \text{ mm}^2$ ) is less than the area of all the individual eyes (Table 3).

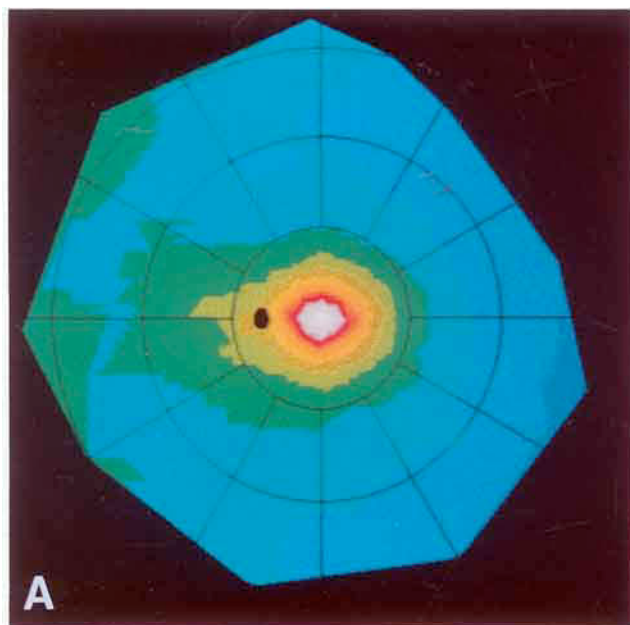
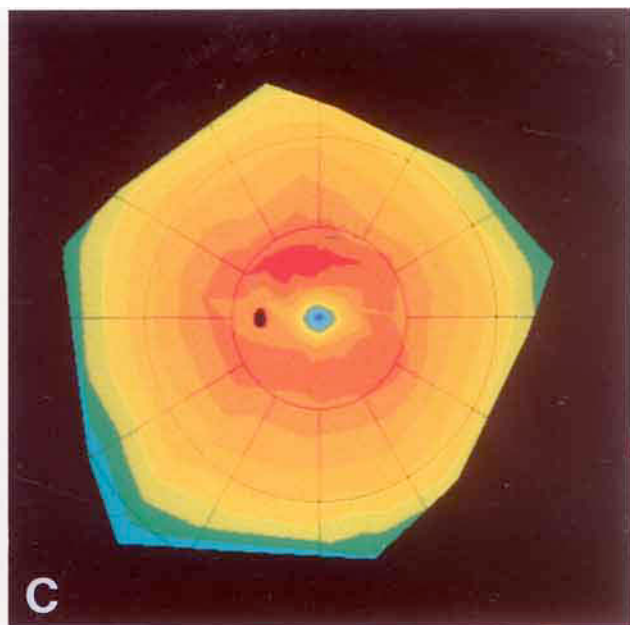
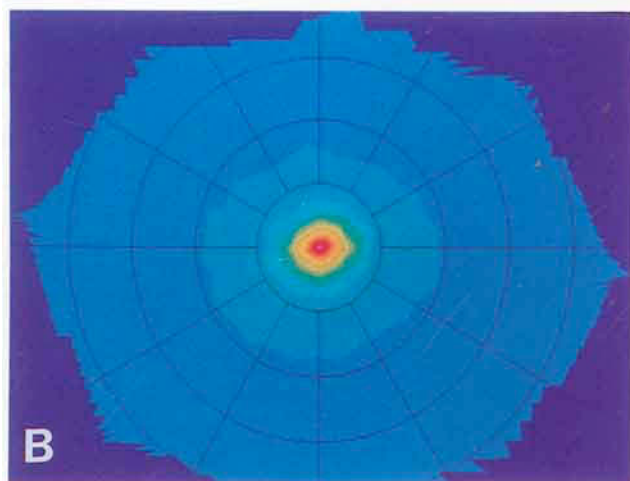
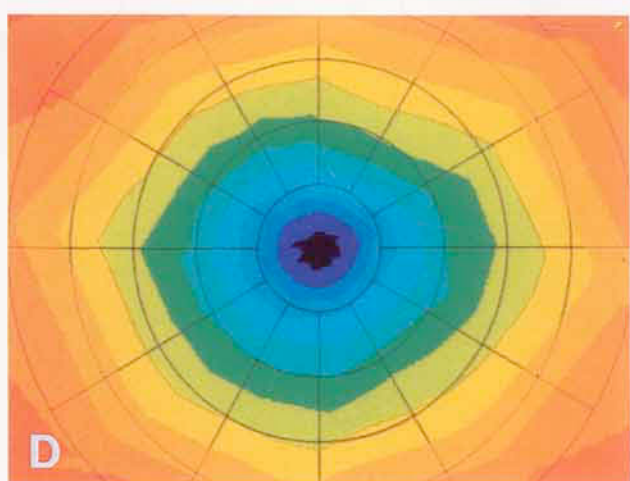
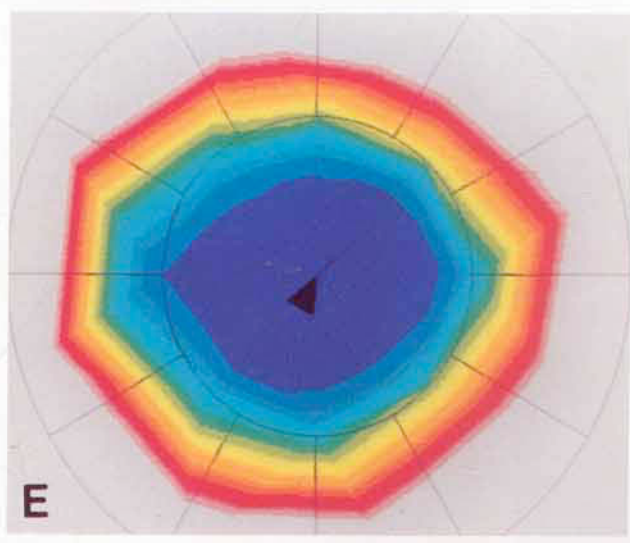
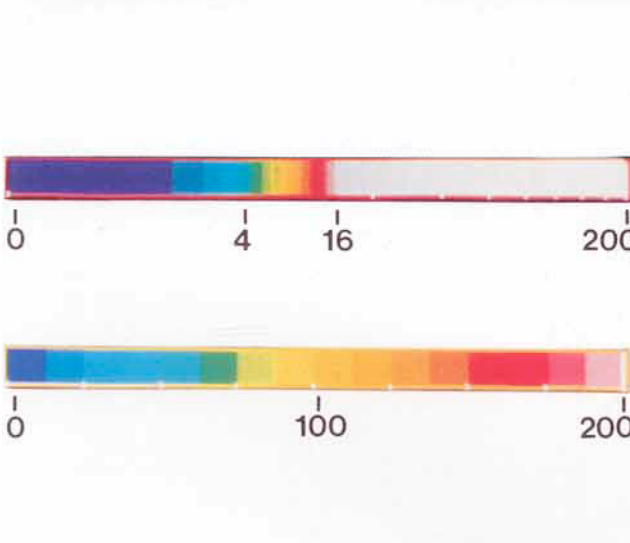
### Conversion to visual degrees

We converted cells/ $\text{mm}^2$  to cells/ $\text{deg}^2$  using Drasdo's and Fowler's ('74) curves for retinal eccentricity and areal magnification, scaling retinal arc length in millimeters from their estimated retinal radius of 11.06 mm and ignoring the angle alpha ( $5^\circ$ ) between the posterior poles of the optic and visual axes. Since this schematic eye is based on average ocular dimensions, the calculated areal magnification factors (ranging from  $0.0795 \text{ mm}^2/\text{deg}^2$  at the fovea to  $0.0379 \text{ mm}^2/\text{deg}^2$  at  $80^\circ$ ) were applied to mean photoreceptor densities only; magnification factors may vary substantially between individual retinas (Holden et al., '87).

## RESULTS

### Appearance of the photoreceptor mosaic in optical sections

For orientation, Figure 1 compares vertical histological and en face optical sections through photoreceptors in the

**A****C****B****D****E**

fovea and midperiphery of human retina. The level of the optical sections is through the ellipsoid portion of the inner segment (arrowheads in Fig. 1A,C), which is just sclerad to where individual inner segments are optically separate. All profiles in the foveal picture (Fig. 1B) are cones. In the periphery (Fig. 1D), large profiles are cones, and small intervening profiles are rods. Ambiguous profiles could be identified by comparing their cross-sectional diameters at several focal planes to those of other cells of certain identity. At any retinal location, rods are always smaller than cones.

Figure 2A,C shows the photoreceptor mosaic in the fovea and perifovea of three eyes. The foveal center, defined as the point with highest cone density, is shown for eyes H5L (Fig. 2A), H4 (Fig. 2B), and H6 (Fig. 2C). Striking differences in density are apparent in that H6 has much smaller and more densely packed cones than the other two. In addition, there were differences in the morphology of cones in H6. The level of focus in Figure 2C is much further sclerad to the ELM than in Figure 2A,B because the great length of the cone inner segments in H6 prevented viewing of levels nearer to the ELM with the 100 $\times$  objective; the integrity of the ELM was verified at 40 $\times$  in this eye. In all three eyes, foveal cones are packed in a lattice which is approximately triangular on

a local scale, with the exception of more disordered patches in the exact foveal center of H4 and H5L. There are also larger-scale variations in packing order, such as the curvature of rows of cones and abrupt changes in the orientation of adjacent rows. Cone inner segments are polygonal in cross section at this level of focus; their equivalent diameter is 2.2  $\mu\text{m}$  and 1.6  $\mu\text{m}$  for the foveal centers of H4 and H6, respectively. The intervening zone of extrareceptoral space is small. The identity and precise location of the dark and light particles between cone profiles in H4 is unknown at present.

Eccentricity-dependent variations in photoreceptor density and size within the fovea itself are also shown for H4 in Figure 2 (D–F). Where rods first intrude into the cone mosaic (Fig. 2D, arrowhead), at 100–200  $\mu\text{m}$  from the foveal center, cones are much larger, about 3.3  $\mu\text{m}$ , but still form an orderly array. Where rods and cones are present in equal density (400–500  $\mu\text{m}$  from the foveal center; Fig. 2E), cones are larger still (4.5  $\mu\text{m}$ ) and are three times larger than the rods. The cone mosaic has lost its regular triangular packing at the sites where rods are present. Further away on the foveal slope (Fig. 2F), cones are less numerous but larger yet. Rods are now about four times more numerous than cones, are larger than they were at 500  $\mu\text{m}$ , and have begun to form incomplete rings around individual cones. Cone profiles continue to be polygonal on the side where they abut other cones but have become round on the side where they abut rods.

Changes in the peripheral photoreceptor mosaic are shown in Figure 3, which compares sites at corresponding eccentricities in nasal and temporal retina in eye H5L. At 1.3–1.4 mm from the foveal center (Fig. 3), in the area that Polyak ('41) calls the parafovea, cones are large and round in profile, and rods encircle almost every cone. Peripheral to this point, the major eccentricity effects in photoreceptor size and density are (columns in Fig. 3) 1) the decrease in cone density, which is greater between the parafovea and 5 mm than it is from 5 mm to 16 mm; 2) the slight increase in cone inner segment diameter particularly in temporal retina; 3) the increase in rod density from parafovea to 5 mm and 8 mm; 4) the rod decrease from there to 16 mm; 5) the increase in rod diameter across the entire eccentricity range but most noticeable between 8 and 16 mm; and 6) a change in cone profile shape from round at 1.3–8 mm to elliptical at 16 mm, presumably because cones in the far peripheral retina are tilted towards the exit pupil of the eye (Laties et al., '68) and our optical sections are thus oblique to the long axis of the inner segment. When rods form more than one row between cones, they form a triangular lattice, and their cross-sectional profiles are hexagonal. Rod profiles are not as obviously elongated as cones in the far periphery, nor are they as refractive as cones. Major differences between nasal and temporal retina (rows in Fig. 3) are that 1) cones are more numerous in nasal retina at all the eccentricities shown but more so at 8 and 16 mm; 2) rod density is greater and rod diameter smaller in temporal retina at 5 mm eccentricity; and 3) at both 8 and 16 mm of eccentricity, rods appear to be less numerous and larger in temporal retina than in nasal retina.

One part of the nasal retina which has no equivalent in the temporal retina is the photoreceptor mosaic immediately adjacent to the optic disk (Fig. 4A). Small patches of high cone and low rod density were observed all around the disk. Cone inner segments are large (10  $\mu\text{m}$  in diameter or more), irregularly polygonal, and short. Cone outer seg-

Fig. 5. Computer-generated color-coded maps of mean photoreceptor density in the human retina. All maps are displayed as the fundus of a left eye in the standard perimetric projection (Frisen, '70), in which the fovea is at the center, and the ora serrata at the circumference, of a polar coordinate system. Distances are preserved along meridians and distorted along lines of isoeccentricity (rings in the overlying grid). Nasal is to the left in all figures. Bars at lower left relate color coding for spatial density of photoreceptors (cells  $\times$  1,000/mm $^2$ ). The upper color bar applies to panels A and E and shows the range from 0 to 16,000 cells/mm $^2$  at intervals of 1,000 cells/mm $^2$ . Densities above 16,000 cells/mm $^2$  are represented by white. The lower color bar applies to panels B, C, and D and shows the range from 0 to 200,000 cells/mm $^2$  at intervals of 12,500 cells/mm $^2$ . **A:** Cones in the entire retina. Foveal cone densities are out of the range of this color scale and so are displayed as white. The lines of isoeccentricity in the overlying grid are at intervals of 5.94 mm, and the black oval is the optic disk. Contours within the eccentricity of the disk are roughly circular. Note also the following features of the region of peripheral high cone density called the cone streak: 1) elongation of isodensity contours along horizontal meridian; 2) a displacement of isodensity contours into nasal retina, which increases with eccentricity; 3) slight displacement of contours inferiorly; 4) broadening of contour for 6,000 cones/mm $^2$  (bright green). Nasal retina has a higher overall cone density than temporal retina, including a slight increase near the ora serrata. **B:** Cones in the fovea. Lines of eccentricity in the overlying grid are at intervals of 0.4 mm. Note the rapid and immediate decline in density away from the pinnacle of peak density, so that half maximal density is at 120–150  $\mu\text{m}$  from the foveal center. Isodensity contours are elongated along the horizontal meridian, but much less than is seen in peripheral retina. **C:** Rods for the entire retina. Grid conventions are the same as in A. Note the small rod-free zone at the fovea, the ring of high rod density (rod ring) at the eccentricity of the optic disk, and the decline in rod density on the peripheral flank of the rod ring. Within the rod ring, note 1) the hot spot of highest rod density in superior retina, 2) the elongation of isodensity contours along the horizontal meridian, 3) the more peripheral extension of the ring into nasal retina, and 4) the gulley formed by lower densities formed where the rod ring crosses the horizontal meridian. On the peripheral slope of the rod ring, isodensity contours are generally circular but displaced nasally and superiorly. **D:** Central slope of rod ring. Grid conventions are the same as in B. Isodensity contours are elongated along the horizontal meridian and are displaced inferiorly. Rod density increases most rapidly on the superior side of the rod-free zone and least rapidly along the horizontal meridian. **E:** Rod-free zone. Rod density rises rapidly out of the density range represented by this color scale. Lines of eccentricity in the overlying grid are at intervals of 0.2 mm. The rod-free zone is the area enclosed within the contour for 1,000 rods/mm $^2$  (dark blue). It is slightly elongated along the horizontal meridian and displaced nasally.

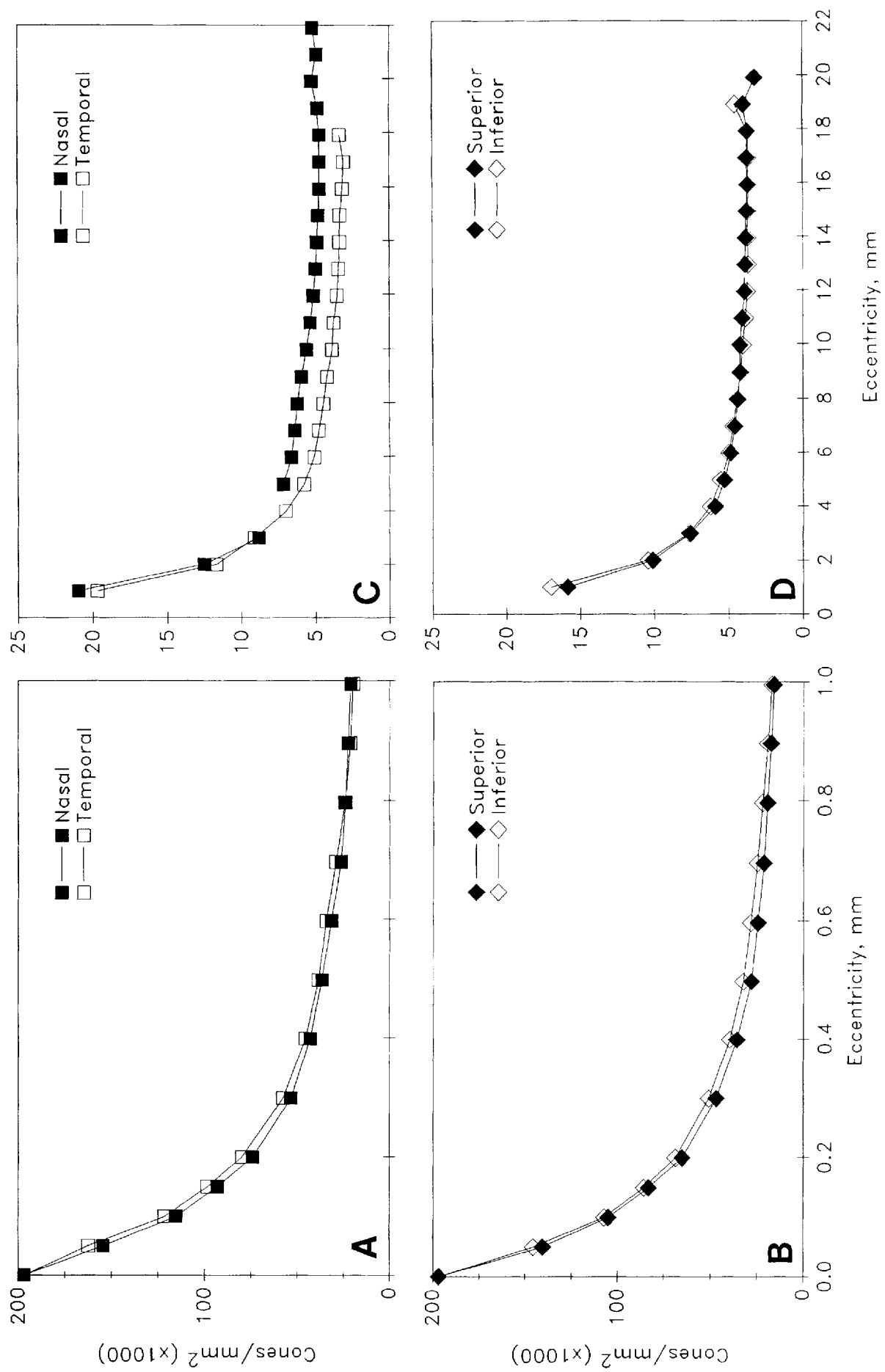
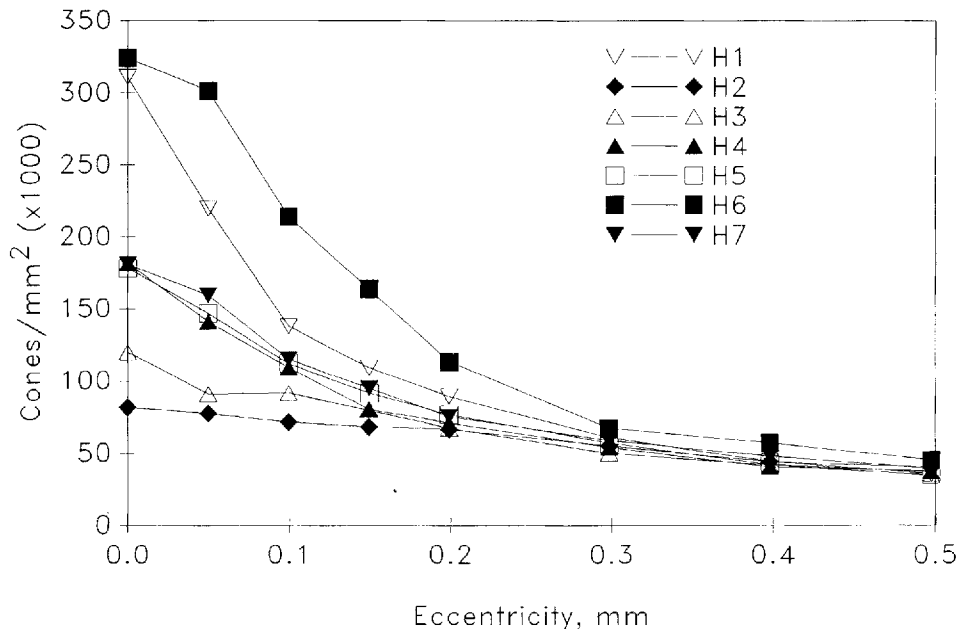


Figure 6



**Fig. 7.** Individual variability in foveal cone density in eight human retinas. Cone density is plotted as a function of eccentricity for the temporal horizontal meridian within 0.5 mm of the foveal center. For illustrative clarity, the mean of the two fellow eyes is shown (H5). The greater than threefold range in cone density at the foveal center effectively disappears by 0.3 mm eccentricity.

ments are also very short. Another part of the nasal retina without temporal equivalent is near the nasal ora serrata at eccentricities greater than the extent of the temporal retina. At 21 mm from the foveal center, the photoreceptor mosaic contains only a few cells in a disordered array (Fig. 4B,C). Cone density is comparable to what was seen at 16 mm nasal (see Fig. 3D), but rod density has continued to decrease. Cones are smaller and elliptical in cross section, and rods are large and elliptical. Because the size difference between rods and cones is smaller than in other parts of the retina, and tissue morphology is often not well preserved, individual rods are generally not countable. Cone inner segments can be distinguished, however, by their greater refractivity and by the granular texture of their mitochondrial array. Finally, the identity of the large cells at 22 mm nasal of H6 (Fig. 4C) is unknown. These cells had no recognizable outer segments and were found anterior to a zone of frank degeneration.

### Topography of cone density

The salient features of human cone topography (Figs. 5A,B, 6) are 1) high peak density in a small area at the foveal center; 2) a steep decrease away from the foveal center, which becomes less steep with increasing eccentricity; 3) a

zone of high cone density ( $>5,000$  cones/ $\text{mm}^2$ ) surrounding the fovea and extending along the horizontal meridian in the peripheral retina (cone streak; Packer et al., '89); 4) higher cone density in nasal retina relative to temporal retina; and 5) slightly increased cone density in the far nasal retina.

**Peak density.** Peak cone density at the foveal center of the average retina is  $199,000/\text{mm}^2$  (Table 3), but between-individual variability was substantial. The addition of more specimens to our previous sample (Curcio et al., '87b) and the calculation of peak density for a smaller counting window has increased the range of peak density to 3.3-fold (98,200–324,100 cones/ $\text{mm}^2$ ). Five of the eight eyes had peak densities exceeding 160,000 cones/ $\text{mm}^2$ , and two were over 300,000 cones/ $\text{mm}^2$  (Table 3). The eye with the lowest peak density, H2, also had an unusually organized fovea, with multilobed isodensity contours and the point of highest cone density displaced 100  $\mu\text{m}$  superior and temporal to the center of the external foveal pit, which was declared to be the foveal center for this case.

If the density gradient is still increasing sharply within our smaller counting window, then it is possible that we have underestimated peak density. In three retinas, peak density was recomputed by excluding cone centers lying outside successively smaller circular windows centered in the standard rectangular window ( $45 \times 29 \mu\text{m}$ ). In retina H4, peak density increased as the window shrank, reaching 212,000 cones/ $\text{mm}^2$  in a circle 9  $\mu\text{m}$  in radius and containing 22 cones, compared to 181,800 cones/ $\text{mm}^2$  in the standard rectangular window. In H5L, density remained within 5% of the density in the standard window. In fact, the peak density of 166,000 cones/ $\text{mm}^2$  in H5L was found in two adjacent windows, and smaller windows centered on the border of the two windows did not increase this value. Thus, the area over which cone density is maximal can vary in size and is poten-

**Fig. 6.** Mean cone density as a function of eccentricity along the horizontal (A,C) and vertical (B,D) meridian. A and B show foveal, and C and D show peripheral cone density at appropriate scales. For this and all other meridian graphs, the symbols represent points where the digital models of the individual retinas were resampled rather than points where data were actually collected (see Materials and Methods for details). The gap at 4 mm nasal (C) represents the site of the optic disk.

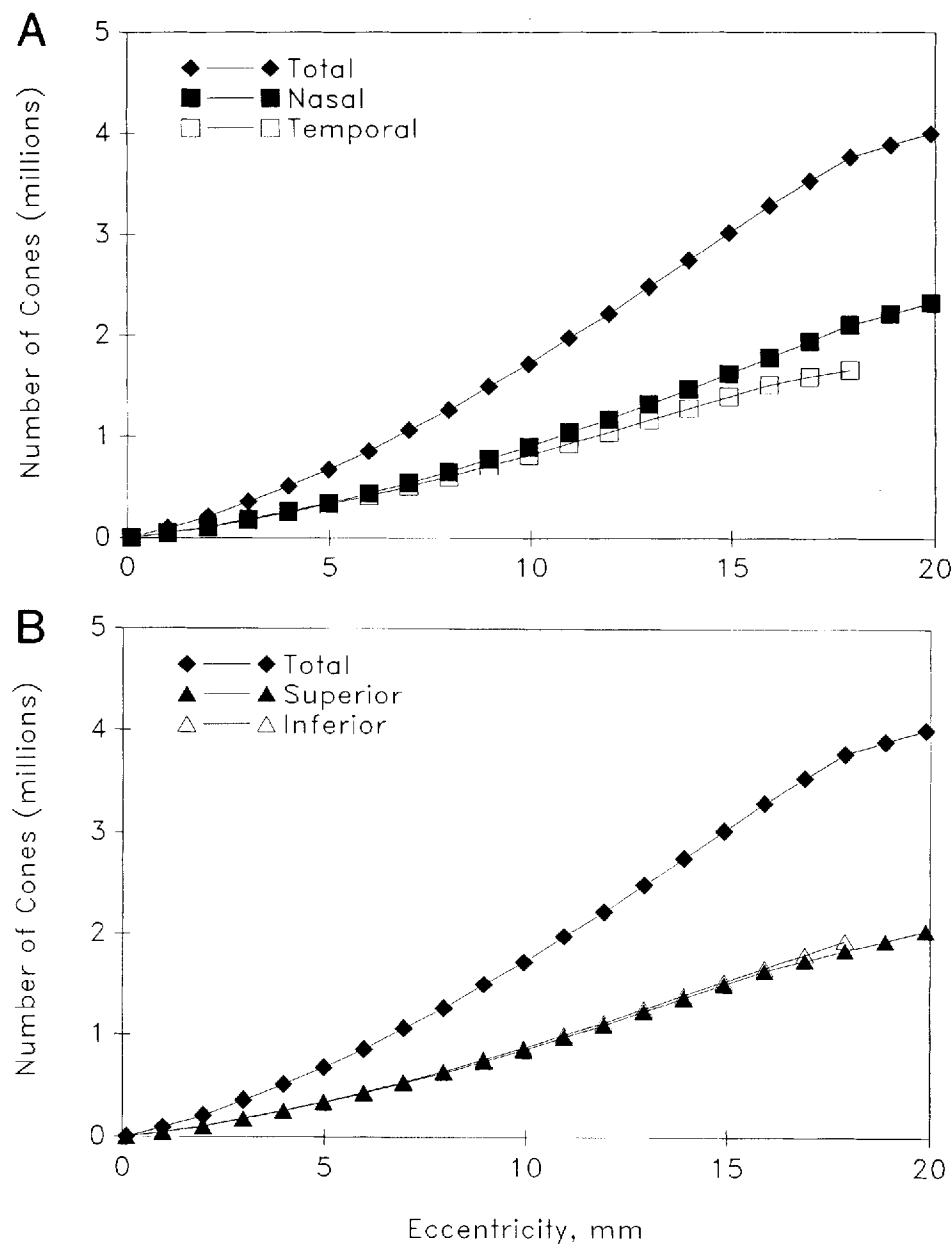


Fig. 8. Cumulative number of cones as a function of eccentricity in mm for an average retina (top curve in A and B), for nasal and temporal hemiretinae (A), and for superior and inferior hemiretinae (lower curves in B). The total number of cones in the entire retina was calculated for disks of ever-increasing radius in a "bullseye" pattern centered on the fovea. For each hemiretina, the total was calculated for half disks split along the appropriate meridian. The total number of cells in the average retina is less than for most individual eyes (Table 3) because locations where there were data from fewer than two eyes were not included.

tially quite large ( $0.16 \times 0.20^\circ$  for two adjacent windows). The extremely high density in the foveal center of H1 (311,000 cones/mm<sup>2</sup>) was maintained across the entire standard window.

**Fovea.** Cone density falls immediately and rapidly away from the pinnacle of peak density such that half-maximum density (at green-yellow contour in Fig. 5B) is achieved only 120 (inferior) to 150 (temporal)  $\mu\text{m}$  from the foveal center. Density along all meridians declines by an order of magnitude, to about 20,000 cones/mm<sup>2</sup>, within 1

mm of the foveal center (Fig. 6A,B). This sharp decline is slightly faster along the vertical than the horizontal meridian in the average eye, resulting in elliptical isodensity contours. Ratios of the distances at which foveal isodensity con-

Fig. 9. Mean rod density as a function of eccentricity in the fovea (A) and along the peripheral horizontal (B) and vertical (C) meridians. The gap in the curve for the nasal horizontal meridian represents the site of the optic disk.

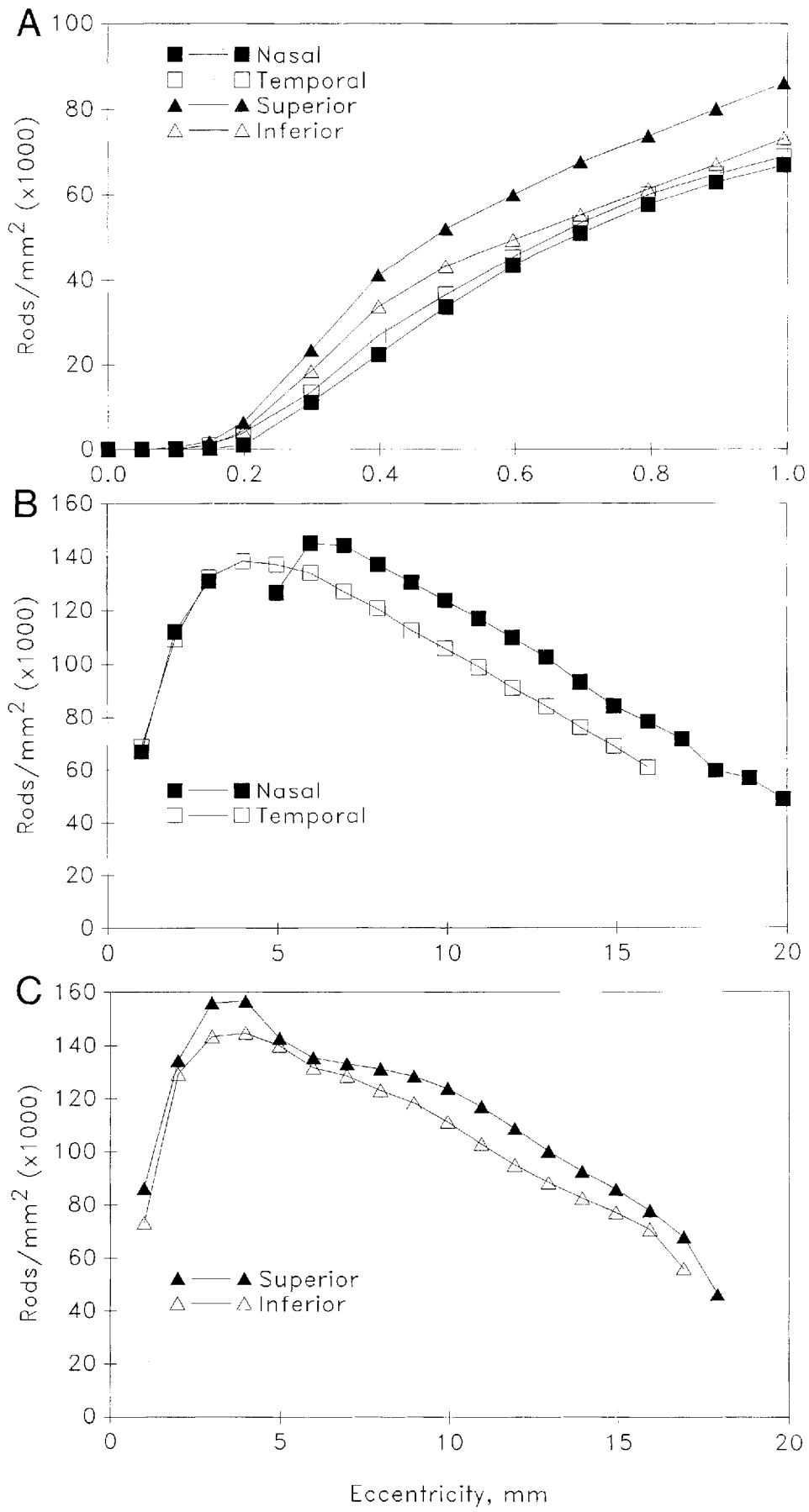


Figure 9

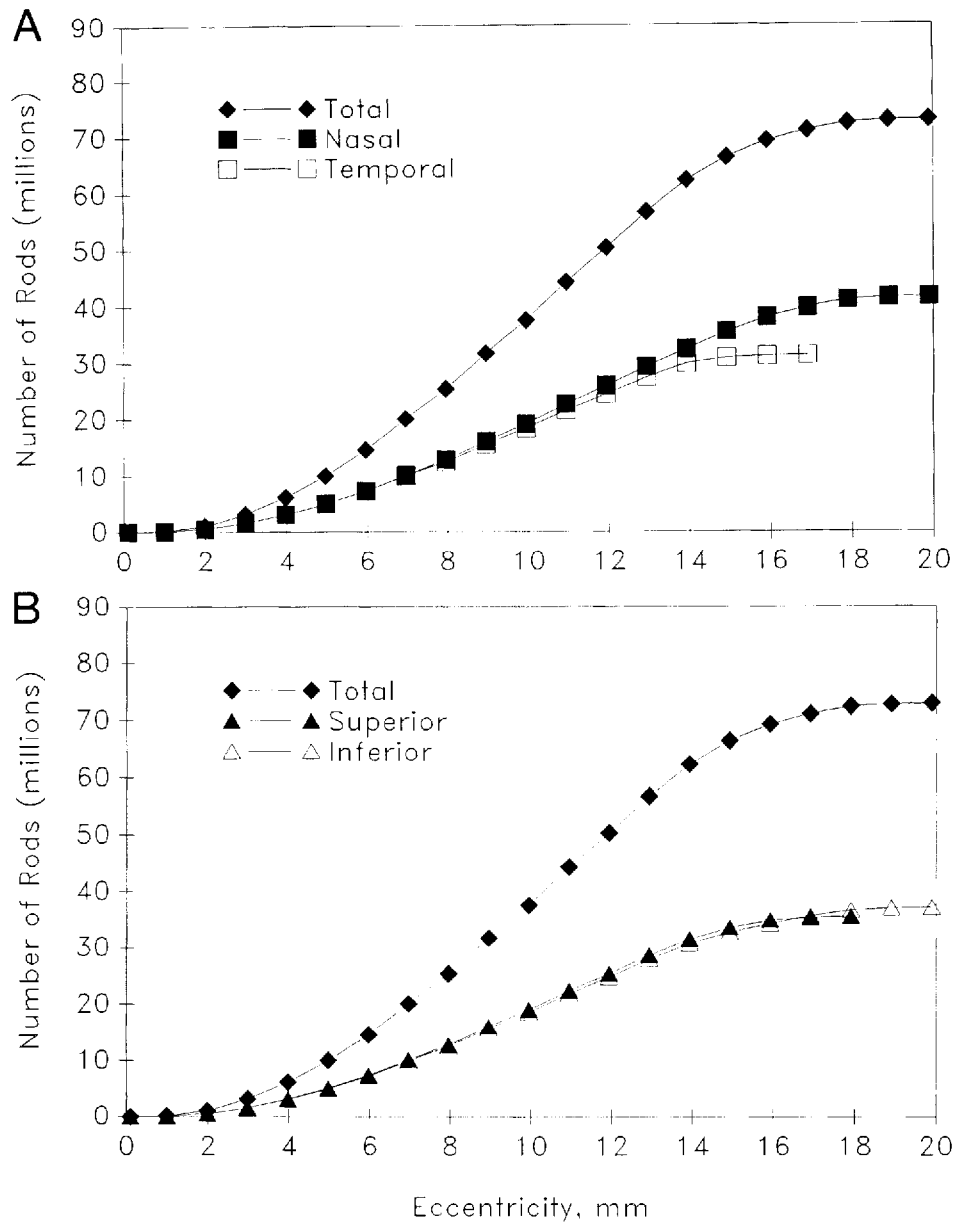


Fig. 10. Cumulative number of rods as a function of eccentricity for the entire average retina (top curve in A and B), for nasal and temporal hemiretinae (A), and for superior and inferior hemiretinae (B). Cumulative curves were generated in the same manner as in Figure 8. The average retina does not extend as far peripherally as some individual eyes, so its total of 80 million rods is lower than the individual eyes (Table 3).

tours crossed the horizontal and vertical meridians (axial ratios) were 1.19–1.22 for the average eye and ranged from 0.92 (almost circular) to 1.67 in individual eyes. The fellow eyes, H5L and H5R, had axial ratios of 1.05 and 1.50, respectively, suggesting that the differences in foveal topography are genuine and not attributable to differences in fixation, since these eyes were obtained and fixed at the same time. Ratios of densities at corresponding eccentricities along the nasal and temporal horizontal meridian (N/T ratio) of the average retina are almost 1.0 from the foveal center to about

1 mm. Curves for cone density in different individuals are spread widely in the foveal center but rapidly become more similar, so that by 0.3 mm eccentricity on the temporal horizontal meridian (slightly over 1° in the visual field), they are tightly clustered (Fig. 7).

**Periphery.** In the peripheral retina (Figs. 5A, 6A,B), the decline in cone density becomes less precipitous and the differences between nasal and temporal hemiretina become more apparent. The most prominent feature in the map is the cone streak, in which isodensity contours are increas-

ingly elongated and displaced into nasal retina with increasing eccentricity. For example, the  $10,000/\text{mm}^2$  contour crosses both the nasal and temporal horizontal meridian at 2.65 mm, but the  $7,000/\text{mm}^2$  contour crosses 33% further away from the foveal center in nasal retina (5.3 mm) than in temporal (4.0 mm). The axial ratio for these two contours are 1.28 and 1.37, respectively. Near 1 mm, nasal retina first begins to show a small numerical superiority over other meridians (Fig. 6A). The N/T ratio at the eccentricity of the optic disk is 1.25, and it continues to increase to values of 1.40–1.45 at 9 mm and beyond. Thus, for much of the periphery, locations in nasal retina have 40–45% more cones per  $\text{mm}^2$  than corresponding locations in temporal retina. In individual eyes, the maximum N/T ratio along the far peripheral horizontal meridian ranged from 1.42 to 2.19; the highest value was found in an eye with particularly low temporal cone density (H5L). The cone streak also extends slightly further into inferior retina than superior retina. Along the vertical meridian of the average retina (Fig. 6D), a ratio between cone densities at corresponding eccentricities in superior and inferior retina ranges from 0.84–0.96 out to 12 mm, then slightly over 1.00 from there to the extreme periphery. The differences between superior and inferior retina were variable in individual eyes and largely canceled out to produce the weak asymmetry in the average. This variability is discussed in greater detail below.

The decline in cone density with eccentricity levels off or turns slightly upward in the far peripheral retina (Fig. 5A, 6C,D). In the contour map, far peripheral isodensity contours ( $5,000 \text{ cones}/\text{mm}^2$ , blue-green; and  $6,000 \text{ cones}/\text{mm}^2$ , bright green) are not elliptical like those at lower eccentricities but instead open up along the vertical meridian and extend to the ora serrata. A slight increase in peripheral cone density starts at 16–18 mm from the fovea in five of the six eyes from which we have data for this eccentricity (Fig. 6C). Cone density at the most extreme eccentricity mapped in nasal retina ranged from 4,700 (H7) to 7,000 cones/ $\text{mm}^2$  (H4), values 13–17% higher than the lowest densities along the nasal horizontal meridian for those two eyes (4,000 and 5,400 cones/ $\text{mm}^2$ , respectively). There are fewer data for the far superior and inferior periphery, and the slight increase in the average graph (Fig. 6D) represents an increase in only one of the three eyes from which we have data for that eccentricity. At eccentricities less than 9–12 mm, temporal retina has more cones than superior and inferior retina; at greater eccentricities, cone density is about 10% lower in temporal retina than superior and inferior retina. Thus no two cardinal meridians are alike across the full range of eccentricities. The overall anatomical central-to-peripheral gradient (in units of cones/ $\text{mm}^2$ ) is 47-fold between the foveal center and 9 mm eccentricity, with an additional 20% decline between 9 and 18 mm. Because 1  $\text{mm}^2$  of peripheral retina subtends a greater visual angle than 1  $\text{mm}^2$  at the fovea (Drasdo and Fowler, '74), the functional central to peripheral gradient (in units of cones/ $\text{deg}^2$ ) is 53-fold between the foveal center (where peak density is 16,000 cells/ $\text{deg}^2$ ) and 32°, with an additional 49% decline between 32° and 68°, the approximate equivalents in the visual field projection.

### Total number of cones

The total number of cones in six retinas ranges from 4.08 to 5.29 million (Table 3). Graphs showing the cumulative number of cones as a function of eccentricity (Fig. 8) reveal that, despite the high density of foveal cones, a disk 400  $\mu\text{m}$

( $1.4^\circ$ ) in diameter centered on the fovea contains about 0.3% of the total number of cones in less than 0.02% of the total retinal area. There are 27% more cones in nasal retina within an eccentricity equal to that of the edge of the temporal retina (Fig. 8A). Since cone numbers in nasal retina continue to accumulate at eccentricities where there is no temporal retina, there are ultimately 39% more cones in the complete nasal retina of the average eye and 17–63% more in individual eyes. Differences in total number (the endpoint of the cumulative curves) reflect both the larger area and the higher mean density of cones in the nasal retina. There are only 2% more total cones in inferior retina than in superior retina throughout most of the periphery of the average eye (Fig. 8B), although the total numbers in the two complete hemiretinas are similar because superior retina is somewhat larger. In individual eyes with complete cone maps and similar area in superior and inferior retina, a 5–14% excess in total cones was found in the inferior retina of three (H4, H5L, H5R), indicating higher mean density in inferior retina. In the other three eyes, the differences between superior and inferior retina in total cone number were similar to the differences in area.

### Topography of rod density

The salient features of the human rod distribution (Figs. 5C–E, 9) are 1) the rod-free zone within the fovea, 2) a ring of nonuniformly high rod density (the rod ring; Packer et al., '89) at the eccentricity of the optic disk, and 3) a slow decrease in density from the rod ring to the ora serrata.

**Rod-free zone.** Rods are absent from the center of the human fovea, first appearing in our counting windows at distances of 100–200  $\mu\text{m}$  from the foveal center. Because our sampling scheme was optimized for the distribution of the more numerous foveal cones, the precise topography of the rod-free zone emerges only in the map of average density (Fig. 5E). The rod-free zone, considered to be the area inside the isodensity contour for 1,000 rods/ $\text{mm}^2$  (dark blue contour in Fig. 5E), is slightly elliptical in shape, with an axial ratio (1.29) similar to cone density contours at the same eccentricity. The rod-free zone is not precisely centered on the point of peak foveal density, since the 1,000 rods/ $\text{mm}^2$  contour crosses the nasal horizontal meridian slightly further away from the foveal center (0.20 mm, or 0.7°) than it did for other meridians (0.12–0.15 mm, or 0.43–0.53°). The horizontal diameter of the rod-free zone is 0.35 mm (1.25°).

**Rod ring.** The highest rod densities are found in a broad, horizontally oriented elliptical ring at approximately the same eccentricity as the center of the optic disk (Fig. 5C). Along the central flank of the rod ring (between the edge of the rod-free zone and the rod ring), rod density increases rapidly with eccentricity to 100,000 rods/ $\text{mm}^2$  within 1.2–1.7 mm of the foveal center (Figs. 5D, 9A). The distribution of central rods is more asymmetric than the distribution of foveal cones in that rod density increases most rapidly along the superior vertical meridian and increases least rapidly along nasal horizontal meridian (Fig. 9A). The exception was retina H3, which had generally lower foveal rod density than the other eyes and the greatest increase along inferior rather than superior vertical meridian. There was significant meridional variation in rod density within the rod ring itself (Fig. 5C, 9B,C). First, the area with highest rod density (the "hot spot") is located in the superior retina. The mean highest rod density was 176,000 rods/ $\text{mm}^2$  and ranged from 157,900 to 188,600 rods/ $\text{mm}^2$  (Table 3). In the average eye (Fig. 5C), the hot spot straddles the superior

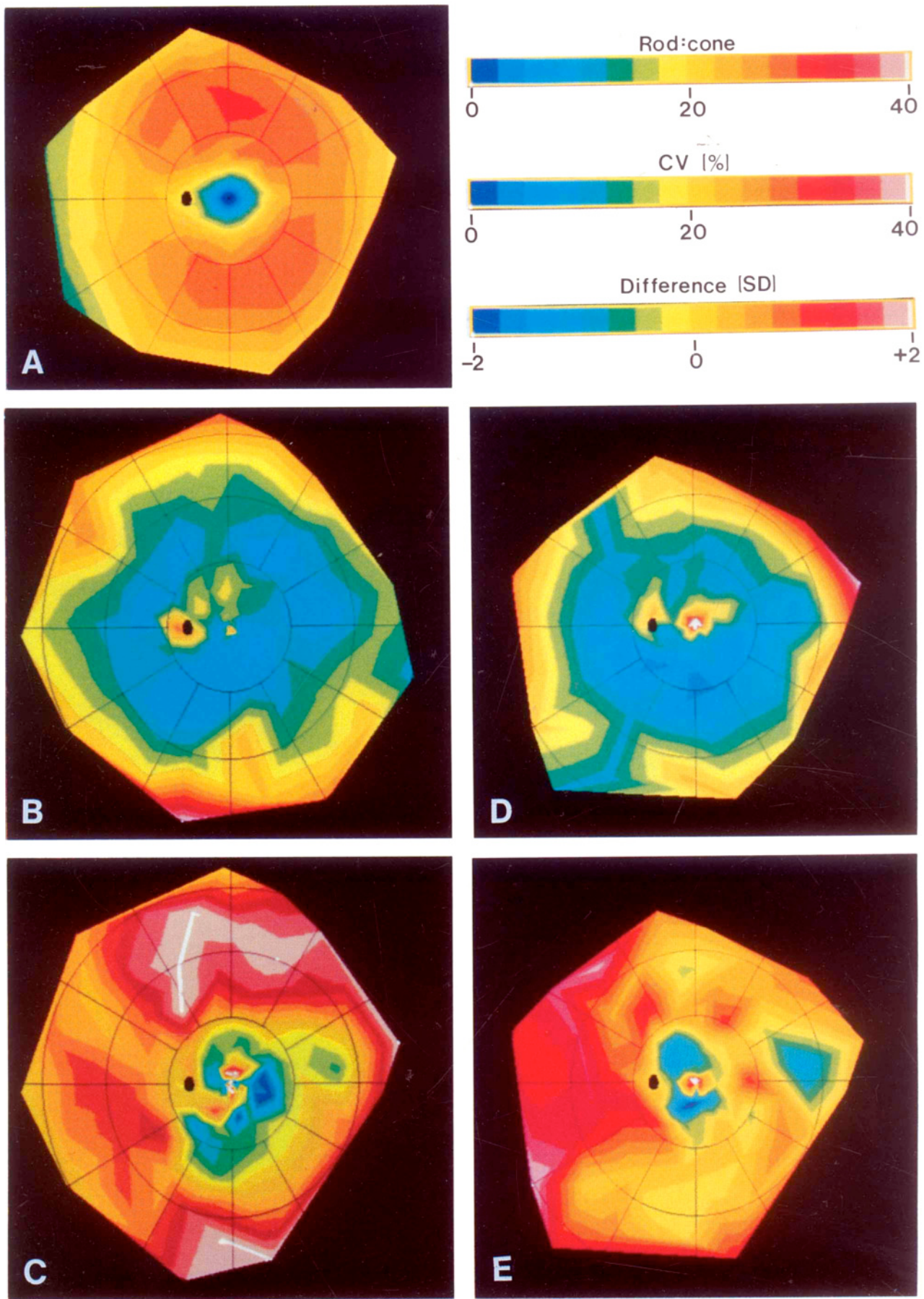


Figure 11

vertical meridian unequally and is mostly in nasal retina. In individual eyes (Table 3), the hot spot was in superior-nasal retina in four eyes, in superior-temporal retina in one eye, and in inferior retina in one (H3). The eccentricity of the rod hot spot was 3–5 mm (Table 3). Second, the ring breaks up into islands in the inferior retina, and the prominence of the inferior part of the ring in Figure 5C is primarily due to the inferior hot spot in H3 and generally high densities in the rod ring of H1. Third, the density of the rod ring is reduced by 15–25% where it crosses both the nasal and temporal horizontal meridian, forming a horizontally oriented gulley of low rod density. In the average eye and all individual eyes except H3, the rod gulley was more prominent nasally than temporally. Finally, the ring extends further into nasal than temporal retina: the highest densities in nasal retina ( $145,000 \text{ rods/mm}^2$ ) are achieved at a greater eccentricity (6 mm) than either temporal (4 mm), superior, or inferior retina (3–4 mm each).

**Peripheral flank of the rod ring.** From the crest of the rod ring, rod density falls off slowly into the far periphery (Fig. 5C). In contrast to the topography of peripheral cones, peripheral rod isodensity contours (fewer than  $150,000 \text{ rods/mm}^2$ ) are roughly circular and displaced towards nasal and superior retina. For example, the  $87,500 \text{ rods/mm}^2$  contour (bright yellow-green in Fig. 5C) has an axial ratio of 0.97 and crosses the horizontal meridian further from the foveal center in nasal retina (14.5 mm) than in temporal (12.4 mm). The highest densities on the peripheral flank of the rod ring are found along nasal horizontal and superior vertical meridians, and densities in temporal retina are always  $15,000\text{--}20,000 \text{ rods/mm}^2$  less than nasal and superior (Fig. 9B,C). The N/T ratio of rod densities exceeds unity at 5–6 mm eccentricity and increases to 1.28 at the point where temporal retina ends. In individual eyes the N/T ratio at eccentricities exceeding 6 mm was as low as 1.0 and as high as 1.72. At eccentricities exceeding 16 mm, rod density declines more precipitously, particularly in superior

and inferior retina. Density continues to decline more gradually in nasal retina, to a minimum of  $49,000 \text{ rods/mm}^2$  at 20 mm.

All retinas had qualitatively similar peripheral rod topography except H3, in which density was highest in inferior retina. Retina H4 had higher mean rod density than other eyes (Table 3): densities dipped below  $100,000 \text{ rods/mm}^2$  only in the far temporal periphery, and this eye had the highest total number of rods (107 million; Table 3). The lowest values for the far periphery were seen in H5L, where rod density dipped below  $30,000 \text{ rods/mm}^2$  in superior retina. Even lower densities are qualitatively present near the ora serrata of this and other eyes (see Fig. 4B,C) but the difficulty in resolving individual rods and the presence of retinal degeneration precluded accurate rod counts in the extreme periphery.

### Total number of rods

The total number of rods in three retinas with complete rod maps ranges from 78 to 107 million (Table 3). The central 6 mm contains the bulk of the highest rod densities but accounts for a one-fourth or less of the total number of rods (Fig. 10A,B). Conversely, the far periphery, which is large in area, contributes little to total number because rod densities are low and are decreasing with eccentricity. Thus, the cumulative curve for rods is considerably more sigmoid in shape than the cumulative cone curve. Within an eccentricity equal to the edge of the temporal retina, nasal retina has 7% more total rods (Fig. 10A). The entire nasal hemiretina has 20–50% more rods than the entire temporal hemiretina in individual eyes. Superior retina has 2% more rods than inferior retina (Fig. 12B).

### Comparison and covariation of cone and rod topography

The ratio of the total number of rods to the total number of cones is 20:1 (Table 3). The local rod:cone ratio is lowest around the fovea, increases to a maximum in the midperiphery, and declines slowly with eccentricity (Figs. 11A, 12). Within the fovea, the rod:cone ratio reaches unity at an eccentricity of 0.4 mm superior and inferior to the foveal center and at 0.5 mm nasal and temporal. In the periphery, the highest average ratios are 30:1 and are found at about 10 mm from the fovea in superior retina. In individual eyes, the maximum ranged from 30.7 to 43.6. The highest rod:cone ratios are found neither where rods are most numerous (along the rod ring) nor where cones are least numerous (at eccentricities exceeding 10 mm in temporal retina). This is because, at the point of highest rod density ( $177,000 \text{ rods/mm}^2$ ), cone densities within the cone streak are still relatively high ( $6,000\text{--}8,000 \text{ cones/mm}^2$ ). From the rod ring to a point 10 mm superior to the fovea, cone density declines to  $4,200 \text{ cones/mm}^2$ , a decline that is relatively greater than the decline in rod density over the same range (to about  $130,000 \text{ rods/mm}^2$ ), so the rod:cone ratio continues to increase with eccentricity. Rod:cone ratios are lowest in nasal retina at all eccentricities, but for different reasons at different eccentricities. Up to the rod ring, rod densities are at their lowest in the nasal retina; at eccentricities exceeding 1 mm, cone densities are relatively high.

The graphs of cone (Fig. 6C) and rod (Fig. 9A) density in the nasal retina have been plotted as though the distributions of both cell types change smoothly and monotonically across the optic disk. However, there are discontinuities in the distributions of both rods and cones in small patches

Fig. 11. Maps of derived parameters and comparisons between eyes. Upper color bar applies to A, middle bar applies to B and D and lower bar applies to C and E. A: Map of average rod:cone ratio in retinas H1–H5R. Each discrete color in upper color bar represents a rod:cone ratio of 2.5, and the range of colors is 0–40. Lines of isoeccentricity in the overlying grid are at intervals of 5.94 mm, and the black oval is the optic disk. Rod:cone ratios are highest in the superior midperiphery and lowest along the central horizontal meridian. B,D: Regional variability in photoreceptor density, depicted in a map of the coefficient of variation (CV, standard deviation/mean) of cone (B) and rod (D) density. Each discrete color in the middle color bar is 2.5%, and the range of colors is 0–40%. In D, CV is undefined in the fovea, where mean rod density is zero and CV was assigned the value of zero. Other conventions are the same as for A. The site of maximum variability in both photoreceptor distributions is in the fovea; for cones, this site is too small to be seen clearly at this scale. Other points of high variability are at the inferior (cones) and temporal (rods) margins, where sample size is small, and near the optic disk, where the narrow rim of high cone and low rod density immediately adjacent to the optic disk was sampled in some but not in other eyes. Variability is lowest in the midperipheral retina. C,E: Maps showing differences in cone density (C) and rod density (E) between our average retina and the specimen analyzed by Østerberg ('35). Differences were computed by sampling the models of both the average retina and Østerberg's data at comparable locations and subtracting our average photoreceptor density from photoreceptor density in Østerberg's. Differences are expressed in units of standard deviation (SD) for our population at each location. The color scale in the lower color bar ranges from  $-2 \text{ SD}$  (Østerberg lower than our mean) to  $+2 \text{ SD}$  (Østerberg higher than our mean) in increments of 0.25 SD. A difference map comparing two nearly identical eyes would be largely yellow and yellow-green.

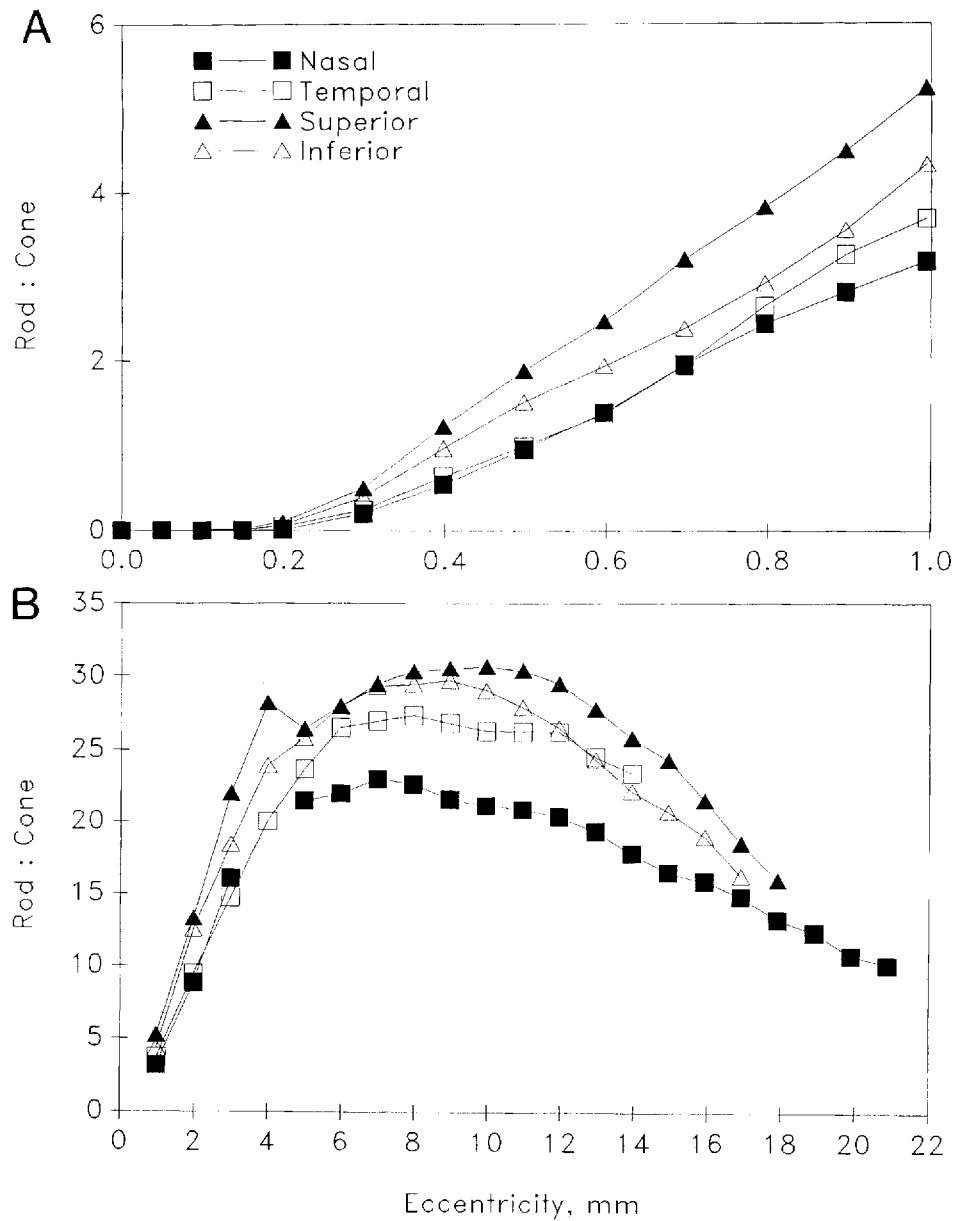


Fig. 12. Average rod:cone ratios as a function of eccentricity along four cardinal meridians, computed from rod:cone ratios in H1–H5R. **A:** Fovea. **B:** Periphery.

immediately adjacent to the disk (Fig. 4A). In a space of 200  $\mu\text{m}$  near the temporal edge of the disk, cone density more than doubles, from  $7,200/\text{mm}^2$  to  $17,000/\text{mm}^2$ , and rod density decreases by almost two-thirds, from  $120,000/\text{mm}^2$  to  $37,000/\text{mm}^2$  (Fig. 13).

As noted above, the superior–inferior asymmetry in cone density was variable between individuals in such a way that cone density appeared to be inversely related to rod density at the same eccentricity. For three of the five eyes with cone and rod maps large enough to include the rod ring (H1, H5L, H5R), cone density was 15–20% lower in the superior part of the rod ring than in the inferior part. For another (H4), cone density was higher superiorly up to the point of the rod

hot spot in superior retina, then was higher inferiorly at eccentricities exceeding that of the hot spot. Finally, for H3, whose highest rod densities were located in inferior retina, cone density was lower throughout the inferior retina than at corresponding eccentricities in superior retina. Because this eye was the only one with this form of superior–inferior asymmetry in cones, we infer that the cone distribution, like that of the rods, is inverted across the horizontal meridian.

#### Between-individual variability

**Cones.** To compare variability in different retinal regions, we created a map showing the coefficient of variation

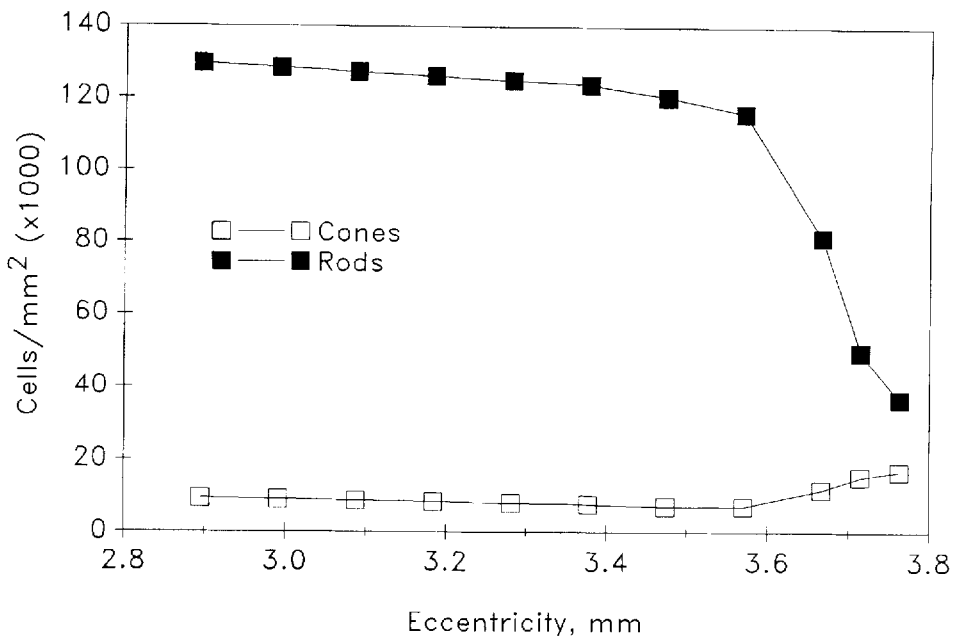


Fig. 13. Spatial density of photoreceptors along the nasal horizontal meridian near the optic disk in retina H4. Eccentricity is shown on an expanded scale. The temporal edge of the disk is just off the right side of the graph, at 3.86 mm from the foveal center. Rod density sharply declines and cone density increases within 200  $\mu\text{m}$  of the disk edge.

(CV; standard deviation/mean) of cone density across the retina (Fig. 11B). The point of maximally variable cone density is at the foveal center, where the CV is 46%, represented by a tiny yellow spot, which is difficult to see at this scale. Variability declines smoothly to 5–17% at 0.3 mm (as also seen in Fig. 7). From there throughout most of the periphery, CV ranges from 8% to 15%, with the least variable densities found at eccentricities of 6–8 mm (medium blue zone in Fig. 11B). Variability is high (30%) around the optic disk, in part reflecting variability in the location of the disk itself. At 10–14 mm from the foveal center, variability increases again, to 19% near the nasal ora serrata and 33–35% in superior and inferior retina. Only at the extreme edge of superior and inferior retina can the increase in variability be explained by a small number of samples. Thus, in contrast to the foveal center, cone density is relatively invariant between individuals over the portion of the retina subserving 1–50° of vision. Different mechanisms may explain the spike of high variability at the foveal center and the slow increase in variability in the far periphery.

If the striking variability in the fovea reflects individual differences in timing, rate, or extent of the lateral migration of cones toward the foveal center during development (Hendrickson and Yuodelis, '84; Youdelis and Hendrickson, '86; Packer et al., in preparation), as previously suggested (Curcio et al., '87b), then eyes with widely varying peak cone density would have a similar number of cones within some distance of the foveal center. Now that we have examined a larger number of human eyes, we computed the total number of cones in circles of increasing radius centered on the fovea (Fig. 14A). Variability in the number of cones within each eccentricity of the cumulative curves in Figure 14A is expressed as a CV (standard deviation/mean) in Figure 14B. The total number of cones within a circle of radius 100  $\mu\text{m}$

centered on the fovea ranged from 2,300 to 6,400, with a mean of 4,100 and a CV of 35%. In contrast, the total number of cones within a circle of radius 1 mm centered on the fovea ranged from 73,600 to 102,700, with a mean of 91,900 and a CV of 10%. In other words, the total number of cones is highly variable between eyes immediately around the foveal center, but, by 1 mm of eccentricity, all eyes have a more similar number of cones, a finding consistent with the developmental hypothesis. Variability in total number continues to decline to a minimum at about 5 mm of eccentricity (Fig. 14B) because the number of foveal cones is a minor contribution to the total number of cones when the extrafoveal retina is included in the total, and cone density in the extrafoveal retina is relatively invariant. In fact, the total number of cones within 14 mm eccentricity is remarkably similar across eyes, about 2.75 million, with a standard deviation of only 5% of the mean. Variability in total number increases at higher eccentricities as retina with more variable cone densities are included in the total.

**Rods.** The overall topography of individual variability in the rod distribution (CV map in Fig. 11D) resembles that of cones, namely, highest variability in the fovea, moderately high variability near the optic disk and the far periphery, and low variability in the midperiphery of inferior retina. In contrast to the cone distribution, however, rods are most variable where they are present in low numbers (from the edge of the rod-free zone to 1 mm eccentricity) and least variable where they are numerous (on the peripheral flank of the rod ring, 3–9 mm eccentricity).

### Within-individual variability

The two fellow eyes of H5 had virtually the same retinal area (Table 3). H5R had higher cone density than H5L

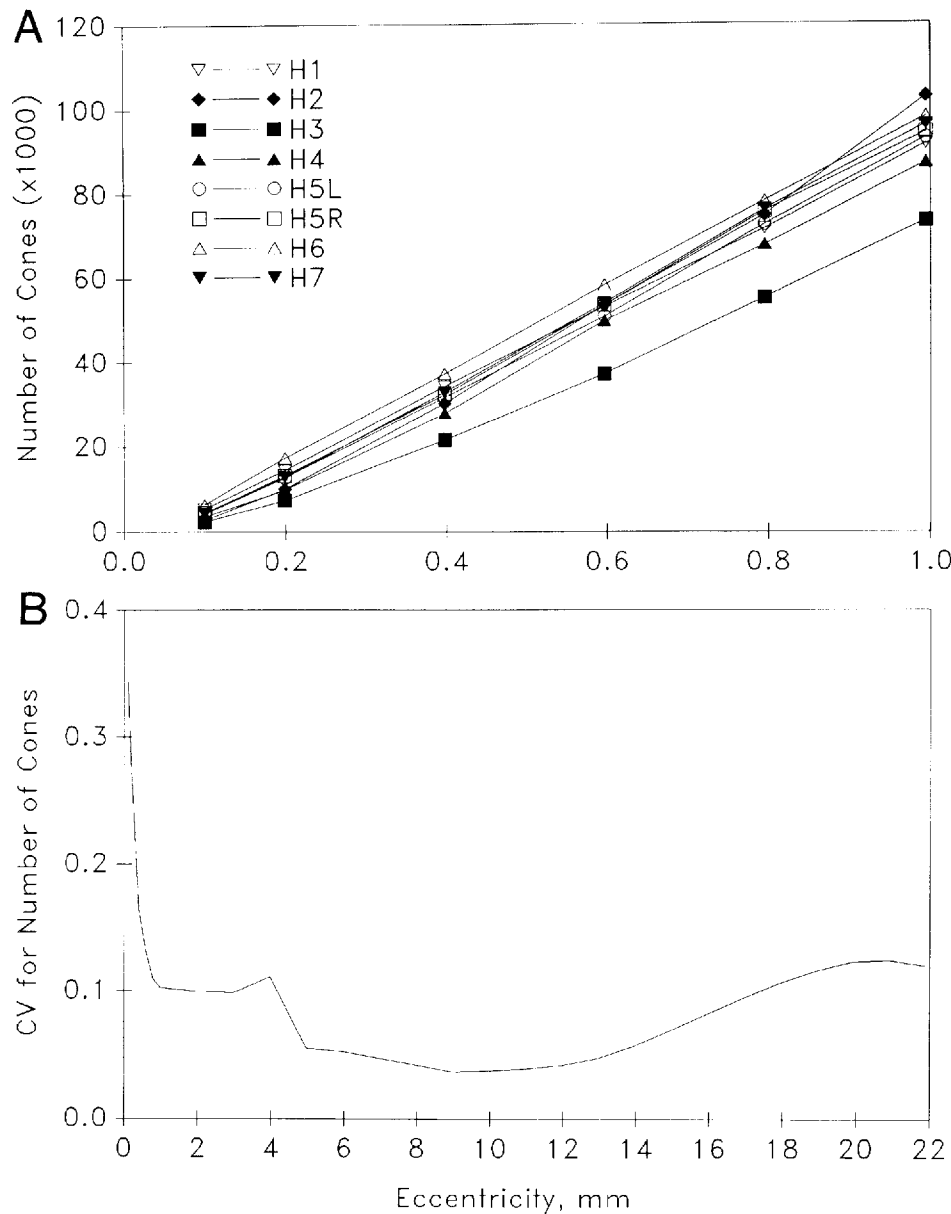


Fig. 14. A: Cumulative number of cones as a function of eccentricity within 1 mm of the foveal center for all eight retinas. This graph was generated in the same manner as the curve for cumulative number of cones shown in Figure 7, except that the increment in radius of disks in the bullseye pattern was 0.2 mm. B: Coefficient of variation (CV, stan-

dard deviation/mean) of the total number of cones as a function of eccentricity for the entire retina. This curve was computed from the cumulative number of cones, for which foveal data only are presented in A. The retinal site with greatest variability in total number is within 1 mm of the foveal center; CV within the central 12 mm is only 5%.

across the entire retina, in spots as much as 30%, and these differences are reflected by the 8% higher number of cones in this eye (4.61 million for H5R vs 4.25 million for H5L). The eyes differed slightly in their peak density of foveal cones ( $190,300/\text{mm}^2$  for H5R and  $166,300/\text{mm}^2$  for H5L). On the nasal side of H5R's fovea, there was a wedge-shaped defect in which photoreceptors were absent, and the remaining retinal layers appear abnormal. In peripheral retina, the cone streaks of the two eyes resembled each other

much more in general shape and orientation than they resembled any other eye, although the right eye had higher densities in the far nasal retina than the left. Within the central 6 mm, the extent of H5R's rod map (Table 2), H5R had 7.8% more rods than H5L. The highest rod density in H5R was higher and was found further from the fovea than for H5L, but H5R had generally lower densities around the rod ring than H5L. Thus, for both rods and cones, fellow eyes have mean densities within 8% of each other. The eye

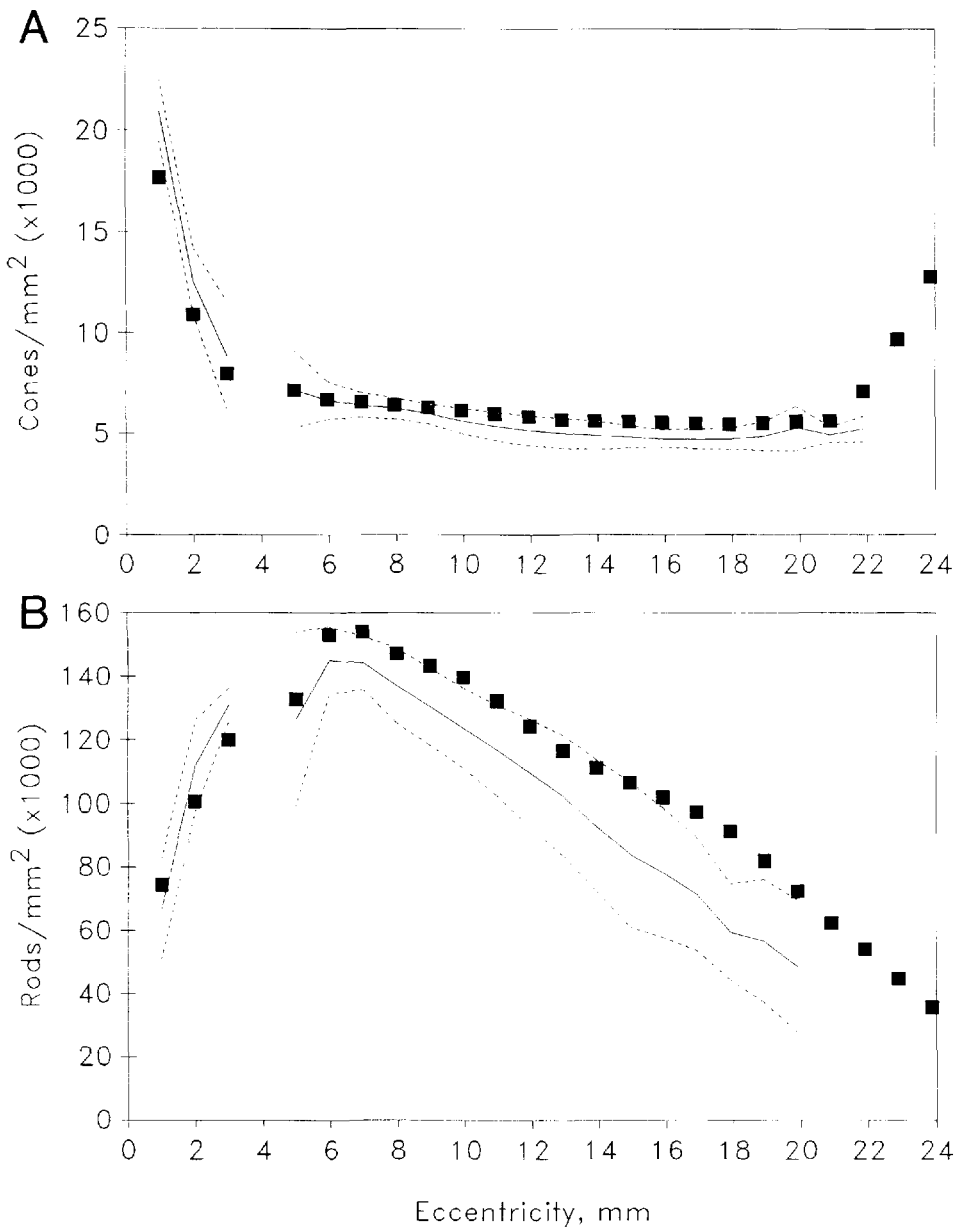


Fig. 15. Comparison of cone (A) and rod (B) density along the nasal horizontal meridian for the average retina (mean: solid line; 1 standard deviation: dashed lines, gap: site of optic disk) and for the specimen studied by Østerberg (squares). The curves begin at 1 mm eccentricity because Østerberg did not sample along this meridian in the fovea.

Østerberg obtained data at greater eccentricities than we did, where he found a marked increase in cone density (A) and a steady decline in rod density (B). For the rest of the peripheral retina, Østerberg's data tend to fall below our mean in the near periphery and well above our mean in the mid- to far periphery.

with higher mean cone density also has higher mean rod density (Table 3). Finally, the topographies of both cell types are similar but not identical in the two eyes.

#### Comparison with Østerberg's data

Because of the importance of Østerberg's ('35) description of the human photoreceptor distribution for vision research over the last half century, we asked whether his single 16-year-old specimen could be considered a representa-

tive eye by comparing a digital model created from his reported photoreceptor densities to the models created for the eyes in this study. Table 3 shows that the mean density (total cells/retinal area) of both cones and rods in the Østerberg eye is within our range but higher than average. In addition, Østerberg's specimen was larger and was sampled at greater eccentricities than any of our eyes, so the digital model of his data encompasses more area. Furthermore, beyond 22 mm in nasal retina (where our data ends), cone density in Østerberg's specimen increases sharply from

5,500 cones/mm<sup>2</sup> to over 16,000 cones/mm<sup>2</sup> (Fig. 15A). At this eccentricity, rod density (Fig. 15B) continues to decline smoothly to values around 35,000 rods/mm<sup>2</sup>; extrapolation of our mean rod density curve to a similar eccentricity results in values around 15,000 rods/mm<sup>2</sup>. The combination of higher densities and larger retinal area results in a higher total number of both cones and rods (6.23 and 110 million, respectively) in Østerberg's specimen than in any of our eyes.

A map of the differences between Østerberg's specimen and our data (in units of the standard deviation [SD] of cell density) at comparable retinal locations reveals that the overall density of cones in mid- to far peripheral retina is 15–40% (more than 1 SD) higher than the our average data, especially in superior and inferior retina (Fig. 11C). There were also isolated patches at 1–2 mm eccentricity, where his density is 30% (almost 2 SD) lower than ours. Like cones, rod density in the periphery of his specimen was higher than our average (Fig. 11E), reaching a maximum of 30–40% (about 1 SD higher) along the superior and nasal edge. Rod densities in temporal retina were close to our mean densities at eccentricities >8 mm. In the fovea, where Østerberg sampled intensively along only the temporal horizontal meridian, the peak density of cones (147,000 cones/mm<sup>2</sup>), measured in a small window (20 × 20 μm), is nevertheless lower than in six of our eight eyes. From 0.15 to 1 mm eccentricity, Østerberg's cone densities are more than one SD unit lower than our mean cone density.

## DISCUSSION

### Overall photoreceptor topography

The fovea is characterized by a high density of cones and the absence of rods in the foveal center, as first recognized by Schultze (1866). We find that cone density declines rapidly with eccentricity, in qualitative agreement with the limited data of Østerberg ('35) for human fovea and the more extensive data for macaque (Rolls and Cowey, '70; Adams et al., '74; Borwein et al., '80; de Monasterio et al., '85; Hirsch and Miller, '87; Schein, '88; Packer et al., '89). This decline is higher along the vertical than along the horizontal meridian. The rapidity of the eccentricity-dependent decrease has come to be appreciated recently in monkey retina, where cone density only 15–20 μm from the foveal center is noticeably lower than the peak (de Monasterio et al., '85; Hirsch and Miller, '87; Schein, '88; Packer et al., '89). In contrast, the area over which the peak density may be considered constant ( $\pm 5\%$ ) in the human retina can be as large as one or two of our standard counting windows. Even this larger area, however, is smaller than the "central bouquet" (100 μm in diameter), which Polyak ('57) describes as containing 2,000 slender cones of similar diameter (and, presumably, of similar density).

The number of cones in the rod-free zone of the average eye is about 7,000, although this number varies considerably between individuals (see below). This may be compared with estimates of 76,282 (within the foveola) and 10,383 (within the central most 250 μm) reported for a 37-year-old eye by Yuodelis and Hendrickson ('86) and 34,000 reported for the rod-free "central territory" by Polyak ('41). Some of this discrepancy is likely due to individual differences and some to differences in how the rod-free zone is defined. The diameter of the rod-free zone is difficult to measure in vertical sections because sections through isolated rod inner segments are easily confused with glancing sections through

cones. Thus our estimate of 350 μm (1.25°) for the horizontal diameter of the rod-free zone is smaller than previous estimates of 500 μm (1.8°) or less for the diameter of the rod-free zone (Polyak, '41) and 683–720 μm for the diameter of the zone devoid of rod nuclei in the outer nuclear layer (Yuodelis and Hendrickson, '86). The latter investigators also noted that the width of the rod-free zone was wider nasally than temporally during development, as we noted in the average adult. Our data are in good agreement with those of Østerberg ('35; replotted by Rodieck, '88), who observed that the density of rods exceeded 1,000/mm<sup>2</sup> at 130 μm temporal to the foveal center. We find that cones decrease, and rods increase, precipitously outside the foveal center such that they are present in equal number at 0.4–0.5 mm, also in excellent agreement with Østerberg ('35).

Although the striking variation of photoreceptor density with eccentricity has long been realized, our new techniques have provided us with a greater appreciation for the richness of meridional variety as well. Peripheral cone density in the midperipheral retina is radially asymmetric, with a horizontally elongated zone of high cone density, the cone streak (Packer et al., '89), surrounding the fovea and extending into nasal retina. The cone streak has three characteristics: 1) a more rapid decline in cone density along the vertical than along the horizontal meridian; 2) 40–45% higher cone density in nasal than temporal retina; and 3) slightly lower cone density in the midperipheral superior retina, near the site where rod density is at a maximum in most eyes. Of these three, the first has been noted for macaque (Perry and Cowey, '85; Packer et al., '89) but not clearly for human (Østerberg, '35); the second has been widely recognized for both human and macaque, although this nasotemporal asymmetry is greater in monkey (Perry and Cowey, '85; Packer et al., '89). The midperipheral superior-inferior asymmetry was first seen by Perry and Cowey ('85), but its relation to rod density at the same eccentricity has been noted only for *Macaca nemestrina* (Packer et al., '89).

We found, in the far periphery, as did Østerberg ('35), that the decline in cone density levels off and even slightly increases as the nasal ora serrata is approached. The meridional specificity of this finding, plus the fact that the declining density of neither rods nor ganglion cells (Allen et al., '89) in the same retinas reaches a similar plateau, argues against differential shrinkage as an explanation. However, we could not confirm the sharp increase to 16,000 cones/mm<sup>2</sup> along the entire nasal rim reported by Østerberg ('35). The human photoreceptor mosaic within 1 mm of the ora serrata contains almost exclusively malformed cones (Hogan et al., '71; Fine and Yanoff, '72), and their spatial density has apparently not been determined by anyone other than Østerberg ('35). It is possible that Østerberg ('35) found this high density because his celloidin-embedded retina was subject to drastic shrinkage at its edges. It is also possible that we missed a zone of very high cone density because we were uncertain of the identity of cells seen at extreme eccentricities (see Fig. 4), or because this zone had been destroyed by microcystoid degeneration, which begins at the ora serrata by age 8 years and progresses posteriorly throughout life (Yanoff and Fine, '82). These changes in cone density in the far and extreme periphery of Østerberg's ('35) specimen have been proposed as compensatory mechanisms for maintaining cones/deg<sup>2</sup> in the face of declining areal magnification (Tyler, '85). However, the modest increase we observed in the far periphery of nasal retina would be insufficient to counteract image compression, and the

TABLE 4. Peak Foveal Cone Densities

Study	Age (years)	Density <sup>1</sup> (cones/mm <sup>2</sup> × 1,000)	Spacing <sup>1</sup> (μm)	Acuity <sup>2</sup> (cycles/°)	Window (μm × μm)	Source of tissue	Methods	
							Shrinkage correction	Preparation
Østerberg ('35)	16	147.4	2.8	58.1	20 × 20	Surgery	Yes	Celloidin, horizontal sections
Hartridge ('50)	n.a.	127.0	3.0	54.3	67 × 58	n.a.	n.a.	Whole mount, dehydrated and cleared
O'Brien ('51)	n.a.	218.3	2.3	70.8		n.a.	n.a.	?; Horizontal sections
		288.6	2.0	81.4				
Miller ('79)	26	128.0	3.0	54.3				Epon, horizontal sections
Yuodelis and Hendrickson ('86)	37	208.2	2.4	67.8		Surgery	Yes	GMA, vertical sections
Farber et al. ('85)	71	119.9	3.1	52.5		Donor	No	
Ahnelt et al. ('87)	47	49.6	4.8	33.9		Surgery	n.a.	Epon, horizontal sections
	72	238.0	2.2	74.0	50 × 50	Surgery	Yes	Epon, horizontal sections
	72	178.0	2.6	62.6		Surgery		
This report	44	311.0	1.9	84.5	43 × 29	Donor	No	Whole mount, DMSO-cleared
	27	98.2	3.4	47.5				
	35	120.0	3.1	52.5				
	34	181.8	2.5	64.6				
	35	166.3 <sup>3</sup>	2.6	61.8				
	35	190.3 <sup>3</sup>	2.5	66.1				
	36	324.1	1.9	86.3				
	32	181.1	2.5	64.5				
Curcio and Allen (in preparation)	37	258.9	2.1	77.1				

<sup>1</sup>Center-to-center spacing if available; otherwise calculated from reported density assuming triangular packing.<sup>2</sup>The period of the highest spatial frequency grating is twice the angular subtense of row-to-row spacing.<sup>3</sup>Fellow eyes.

deranged morphology of cones at more extreme eccentricities makes the possibility of normal visual function unlikely.

Our maps of rod topography represent the first extensive investigations of the human rod distribution since Østerberg ('35). Some of the features of rod topography outside the foveal center, such as the rod ring (with peak density of 170,000 rods/mm<sup>2</sup>), and the higher densities of rods in far peripheral nasal and superior retina, were noted by Østerberg ('35). His data from within the central 2 mm is sparse, however, and thus the asymmetrical distribution of rods within the central slope of the rod ring has not been previously seen in human retina. Neither has the meridional variation of rod densities along the rod ring, and the presence of lower rod densities along the horizontal meridian (although our model of his data reveals such lower densities). The hot spot of highest rod density was superior to the optic disk in Østerberg's specimen, but our maps of additional eyes have shown that the hot spot is a feature in the superior retina of most but not all eyes. These features of the human rod distribution are qualitatively similar to rod topography recently described for *Macaca nemestrina* (Packer et al., '89).

### Variability in foveal cone density

The absolute value of the density of cones at the foveal center is of interest because it is this site that provides the maximum anatomical resolving power for the eye (Helmholtz, '24). We have extended our previous observation (Curcio et al., '87a) that peak foveal cone density is highly variable between individuals. We find that peak cone density ranges from 98,000 to 324,000 cones/mm<sup>2</sup>, the latter being close to what has previously been reported for birds of prey (Miller, '79; Reymond, '85, '87). Our report is the first since that of Fritsch ('08) to include a large number of similarly prepared specimens in a narrow age range. Table 4 shows that there is a greater than sixfold range in estimates of peak density among modern studies. The majority of specimens (9/12) for which the reported age is between 16

and 50 years have peak density in excess of 147,000 cones/mm<sup>2</sup>.

Determining peak density is fraught with methodological difficulties (Packer et al., '89). There are at least three errors that may lead to differences between various studies: 1) misidentification of the foveal center, 2) large counting window, and 3) failure to correct for shrinkage. The first two factors tend to underestimate peak density, and the third tends to overestimate it. We found the foveal center by gross landmarks in the whole mount (such as the foveal depression and the radiating fibers of Henle) and by densely sampling in the rod-free zone to find the site of highest density. Decreasing the area of our counting window increased peak density in some but not all eyes, indicating that the zone of highest density can vary in size. Finally, we are confident that changes in overall tissue volume are minimal, but we cannot dismiss entirely the idea that larger changes may have occurred in just the fovea without information about dimensions of the foveal pit *in vivo*. We sought to minimize these effects by rigorously screening the retinas used in this study. We might expect that the external limiting membrane (ELM) would have been disrupted had the fovea shrunk or swelled more than the surrounding tissue. Because the two low-density foveas (H2 and H3) had more breaks in the ELM than the other eyes, estimates of peak density in these foveas are likely to be underestimates of actual peak density, and the packing geometry of cones in these specimens may be quite different from the situation *in vivo*. Furthermore, H2 alone had a multilobed density distribution, with no obvious peak. Even if these two eyes are not considered, the overall range of the remaining eyes in our sample is still almost twofold (166,000–324,000 cones/mm<sup>2</sup>). The two high-density foveas (H1 and H6) were characterized by an intact ELM and cones with very long inner segments. Although it is possible that tissue shrinkage could explain the high cone density observed in these foveas, it is unlikely to explain the difference in cone morphology.

For the human retina, we need to consider the effects of additional factors on peak cone density. First, a variable interval of postmortem delay before fixation may introduce

differences in shrinkage or quality of preservation, but our rapidly fixed surgical specimen did not have better morphology than the donor eyes. Furthermore, recent reports with use of our retinal whole-mount technique (Hawken et al., '88; Wikler et al., '88; Packer et al., '89) have indicated that the macaque retina, which can presumably be fixed more rapidly than human, also exhibits a large range of peak cone densities (6.9-fold range for  $n = 8$ , Hawken et al., '88; 2.4-fold range for  $n = 7$ , Wikler et al., '88; 1.4-fold range for  $n = 3$ , Packer et al., '89). Second, since human eyes are more likely to be obtained from elderly donors, age-related loss of photoreceptors (Gartner and Henkind, '81) is possible. There were no obvious age trends in our data; the oldest specimen (H1, 44 years) had one of the highest, and the youngest (H2, 27 years) had one of the lowest peak densities.

Variability in the human fovea was also noted in the remarkable study of Fritsch ('08; summarized by Österberg, '35), who reported observations on a collection of 175 histological specimens collected from individuals around the world. Fritsch noted that the diameter of cone inner segments in the central bundle of the fovea varied from 1.8 to 4.5  $\mu\text{m}$  between individuals. If we assume that these cones form a triangular lattice (Snyder and Miller, '77; Miller, '79; Hirsch and Hylton, '84b; Hirsch and Curcio, '89) and that cone inner segments occupy 82% of the distance between their centers (Miller and Bernard, '83; Curcio, in preparation), these diameters correspond to a greater than sixfold range in densities, from 38,000 to 240,000 cones/mm<sup>2</sup>. Fritsch also noted the inverse relation between cone inner segment area and cone density, such that slender cones were also close together. However, wide gaps separated the larger cones of the lowest density foveas. It is likely that these specimens were also disrupted by disease, age, or postmortem tissue processing, as pointed out by Polyak ('41), so the low end of this large range is probably artifact.

### Mechanisms underlying between-individual variability

Our investigation of regional between-individual variability in photoreceptor topography revealed that cone density outside the central 0.3 mm is relatively invariant, with variability at its minimum between 5 and 14 mm of eccentricity. Thus, within the central 5 mm, all retinas have approximately the same number of cones distributed differently. Rods are also highly variable in their foveal distribution and are least variable over approximately the same range as the cones. Here we consider how this pattern may reflect the developmental history of the photoreceptor mosaic.

It is important to determine if the sites of high individual variability reflect merely limitations in our methods of sampling, reconstruction, and analysis rather than real biological variation. Among these methodological explanations is an inadequate number of specimens in our sample. This is likely to be true at the extreme periphery only, since the maps include data only from the largest retinas at those eccentricities. Conversely, the maximum number of eyes was included in the fovea, where variability in both rods and cones is highest. Inadequate sampling within a retina is the likely case for foveal rods, which are present in low density, and thus individual rod maps are very noisy in this area. Noncomparable sampling across different retinas is the likely explanation for the patch of higher variability in the density of both rods and cones around the optic disk, since

the position of the disk itself is variable. Finally, we may have introduced variability by comparing densities from different eyes at the same proportional rather than absolute distances from the fovea. In other words, our digital model assumes that retinas can be uniformly scaled. To check this assumption, we compared densities from different eyes at the same absolute distance from the fovea (nonuniform scaling). Maps of the CV for the nonuniformly scaled model were almost identical to those for the uniformly scaled model for both rod and cone density, indicating that our reconstruction process did not introduce substantial variability. Thus methodological problems do not explain the high variability of foveal cones, the variability minima in midperiphery for both rods and cones, and the slow increase in variability in both rods and cones from mid- to far periphery.

We previously offered two speculations (Curcio et al., '87b) to explain the remarkably three-fold range in peak foveal cone density. First, variability in foveal cone density may be related to variability in optical constants of individual eyes to maintain constant image magnification on the retina. If this is the case, then it is puzzling why photoreceptor densities in extrafoveal retina are not equally variable, since approximately the same retinal magnification factor (mm/ $^{\circ}$ ) applies to the central 30° of vision (Drasdo and Fowler, '74). We cannot address this issue without more information about axial length and other optical parameters than is available for donor eyes. Second, the variability in foveal cone density may be related to variability in rate, timing, or extent of retina involved in the migration of cones during development (Hendrickson and Yuodelis, '84; Yuodelis and Hendrickson, '86). This hypothesis is supported by our finding that the total number of cones within 1 mm has a 1.4-fold range compared to a three-fold range within 0.1 mm. Thus eyes with widely varying foveal cone densities have a similar number of cones, which have been distributed differently.

We have recently studied development of the photoreceptor mosaic in the retina of the macaque (Packer et al., '88, in preparation), a species whose mosaic qualitatively resembles that of humans. We found that the density of foveal cones and rods increased and that of peripheral cones and rods decreased over the period from 2 weeks prenatal to adulthood. The best explanation for these phenomena was lateral migration toward the foveal center and ocular growth in the periphery. In the midperiphery, just beyond the eccentricity of the optic disk, the effects of those two developmental mechanisms could not be dissociated because they are either absent or in equilibrium. It is striking that the zone of minimum variability in the distribution of both cones and rods that we find in this study is roughly the same as the zone least affected by the two major developmental forces. Beyond the midperiphery, variability in the density of both cones and rods increases again, presumably reflecting individual differences in postnatal ocular growth. Therefore, we restate our hypothesis: differences in developmental processes are reflected in variability between individuals at the same stage of development. In this study, we assume that all the eyes have finished development (Yuodelis and Hendrickson, '86) but are not yet subject to possible senescent changes (Gartner and Henkind, '81).

Developmental variability is perhaps best exemplified by retina H3, whose rod and cone maps were both inverted dorsoventrally but whose nasotemporal asymmetries appeared to be similar to those of the other retinas. The overall radial

asymmetries in the topography of cones and rods are present at 2 weeks before birth in the macaque (Packer et al., in preparation). The finding of a retina like H3 suggests that certain developmental specifications of photoreceptor topography, such as the dorsoventral axis, arise from factors external to the photoreceptors and common to both cones and rods. Other specifications, like the nasotemporal asymmetry, may be specific to particular cell populations, perhaps at the level of cell generation.

### Relation of photoreceptor topography to visual function

**Cones.** Foveal cone spacing is commonly assumed to be the limiting factor of visual resolving power. Resolution of gratings consisting of alternating light and dark bars requires that at least one row of unstimulated cones lie between rows of stimulated cones (Helmholtz, '24). We calculated angular cone spacing from our density measurements, using reasonable assumptions about cone packing geometry (Miller, '79) and ocular optics, and compared these values to behaviorally determined measures of human resolution acuity. A more formal comparison has been made between acuity and directly measured cone spacings across the fovea of H4 (Hirsch and Curcio, '89). Here we restrict our considerations to the foveal center.

Table 4 shows that the mean acuity predicted from foveal cone density in our sample of retinas is 66.3 cycles/ $^{\circ}$ , with a range of 47.5–86.3 cycles/ $^{\circ}$ . Both the mean and the range are of interest. First, comparisons of optical quality and the foveal cone mosaic (see, e.g., Snyder et al., '86) have concluded on the basis of the previously available, relatively low estimates of foveal cone density (Østerberg, '35; Miller, '79) that the cone mosaic is well designed to sample the highest frequencies passed by the ocular optics, about 60 cycles/ $^{\circ}$  (Campbell and Gubitsch, '66). Our finding of generally higher density foveas suggests that the foveal cone mosaic may be capable of resolving somewhat higher frequencies. Second, foveal visual acuity is highly variable, ranging from 30–60 cycles/ $^{\circ}$  even in highly practiced psychophysical observers (Weymouth et al., '28; Ludvigh, '41; Weiskrantz and Cowey, '63; Sloan, '68; Westheimer, '82; Hirsch and Curcio, '89, for summary). These studies used a variety of stimulus configurations and luminance levels, and it may be assumed that some variation is purely methodological in origin. Nevertheless, if foveal cone spacing were the only factor underlying foveal acuity, then this twofold range in acuity would require a fourfold range in cone density, compared to the 3.2-fold range we actually observed. These data are not inconsistent given the precision of the acuity estimates, but factors other than cone spacing are most likely involved in producing the functional variability.

These discrepancies can be resolved only with detailed anatomical and functional information from the same eyes, a conjunction of events that may be possible only with animal models. The one eye for which we do have some information about visual function *in vivo* is the surgery case, H7. This retina had a peak density of 181,000 cones/mm $^2$  (for a predicted acuity of 55.8 cycles/ $^{\circ}$ ), compared to a Snellen acuity of 20/20 (or 30 cycles/ $^{\circ}$ ). However, performance may not have been optimal, since patients often are not tested for visual acuity better than 20/20.

Qualitatively, lines of isoacuity within 1.5° of fixation (Weymouth et al., '28) are centered on the foveal center, elongated along the horizontal meridian (axial ratio of about

2), and displaced slightly into inferior retina. This description is not very different from the picture of foveal cone densities (Fig. 7B). At greater eccentricities, isoacuity contours differ from cone isodensity contours in the degree of displacement into nasal retina (and, hence, in the degree of difference between nasal and temporal hemiretina), the presence of a superior-inferior asymmetry that is greater and opposite in direction to the mild asymmetry in the cone distribution, and the lack of increased acuity as far out as 90° in the nasal retina (Wertheim, '80). The lines of isoacuity in fact more closely resemble the distribution of ganglion cells (Curcio and Allen, in preparation), which is not surprising because of the increased convergence of cones onto individual ganglion cells in the peripheral retina.

Given the difficulty in direct comparisons of retinal anatomy and spatial vision, perhaps a more straightforward comparison can be made between our data and laser interferometric measurements of cone spacing *in vivo*. Williams ('88) has recently reported that the minimum row-to-row spacing of cones in eight observers falls between 0.51 and 0.57 min arc, which corresponds with densities of 151,000 and 121,000 cones/mm $^2$ , respectively, a range that is narrower and lower than our range for peak cone density. Foveal cone spacings measured psychophysically are generally larger than those measured anatomically (see Williams, '88, Fig. 4, where his data and data from H1–H4 are compared directly). However, the topography of foveal cone spacing measured psychophysically (Williams, '88) resembles that measured anatomically: Cone isospacing contours are centered around a minimum at the foveal center and are either circular or slightly elongated along the horizontal meridian. In the periphery, cone spacings deduced from the spatial frequency at which interference fringes appear to reverse their orientation (Coletta and Williams, '87) agree well with mean cone spacing derived from our anatomical estimates of spatial density.

**Rods.** The vision mediated by rods at low light levels is characterized by poor spatial resolution and high sensitivity. Because of the extensive convergence of rods onto postreceptor cells, the width of the rod bipolar receptive field is likely the limiting factor in scotopic acuity rather than the spacing of rods themselves (Rodieck, '88). As for scotopic sensitivity, it is commonly assumed that a retinal site with high density of rods is more sensitive than a site with low density. This assumption is qualitatively valid, in that maximum sensitivity to light is found at 20–30° of eccentricity, corresponding to the rod ring (Pirenne, '67). Furthermore, Pulos and Bresnick ('88) have recently shown that scotopic sensitivity along the temporal horizontal meridian forms an inverted-U function resembling that of rod density. They found that sensitivity increased 4.7-fold from 2.5° to 20°, an eccentricity range over which rod density increases 2.6-fold. Within central retina, Crawford ('77) reported for one human observer a roughly circular area of depressed sensitivity centered on a minimum at the foveal center, a topography resembling that of central rods. These data also indicate that, over a narrow eccentricity range (1–2°), sensitivity increases faster than rod density. Better understanding of the quantitative relations of rod density to sensitivity across the retina will require more extensive information about regional differences in scotopic sensitivity as well as information about factors such as photoreceptor coupling and convergence onto rod bipolars, both of which can serve to improve signal-to-noise ratio under appropriate circumstances (Tessier-Lavigne and Atwell,

'88). Nevertheless, we may speculate that the rod ring could be a way of placing the maximum number of rods near but not in the foveal center, a site reserved for the maximum number of cones. Likewise, the significance of the more subtle meridional variation in rod density around the rod ring, such as the rod gulley, may be related to preserving the horizontal meridian for the cone streak. The site of highest rod density in superior retina may be significant for improving sensitivity in the lower visual field, perhaps for viewing the foreground or the hands in dim light.

### ACKNOWLEDGMENTS

We thank Douglas McCulloch and Kimberly Allen for excellent technical assistance in all phases of this project and Kim Graybeal for assistance in manuscript preparation. We also thank the personnel of the Lions Eye Bank at the University of Washington for their cooperation and diligence in obtaining tissue. We are grateful to Drs. Orin Packer and Joy Hirsch for their comments on the manuscript. This work was supported in part by NIH grants EY06109 (C.A.C.), EY01208 and EY04536 (A.E.H.), CORE grant EY01730 and funds from Research to Prevent Blindness to the Department of Ophthalmology, and the Lions Sight Conservation Foundation of Washington and Northern Idaho.

### LITERATURE CITED

- Adams, C.K., J.M. Perez, and M.N. Hawthorne (1974) Rod and cone densities in the rhesus. *Invest. Ophthalmol.* 13:885-888.
- Ahnelt, P.K., H. Kolb, and R. Pfug (1987) Identification of a subtype of cone photoreceptor, likely to be blue sensitive, in the human retina. *J. Comp. Neurol.* 255:18-34.
- Allen, K.A., C.A. Curcio, and R.E. Kalina (1989) Topography of cone-ganglion cell relations in human retina. *Invest. Ophthalmol. Vis. Sci.* 30[Suppl]:347.
- Ahumada, A.J., and A. Poirson (1987) Cone sampling array models. *J. Opt. Soc. Am. A* 4:1493-1502.
- Borwein, B., D. Borwein, J. Medeiros, and J.W. McGowan (1980) The ultrastructure of monkey foveal photoreceptors, with special reference to the structure, shape, size, and spacing of the foveal cones. *Am. J. Anat.* 159:125-146.
- Bunt-Milam, A.H., J.C. Saari, I.B. Klock, and G.S. Garwin (1985) *Zonula adherentes* pore size in the external limiting membrane of the rabbit retina. *Invest. Ophthalmol. Vis. Sci.* 26:1377-1380.
- Campbell, F.W., and D.G. Green (1965) Optical and retinal factors affecting visual resolution. *J. Physiol. (Lond.)* 181:576-593.
- Campbell, F.W., and R.W. Gubitsch (1966) Optical quality of the human eye. *J. Physiol. (Lond.)* 186:558-578.
- Coletta, N.J., and D.R. Williams (1987) Psychophysical estimate of extrafoveal cone spacing. *J. Opt. Soc. Am. A* 4:1503-1513.
- Crawford, M.L.J. (1977) Central vision of man and macaque: cone and rod sensitivity. *Brain Res.* 119:345-356.
- Curcio, C.A., O. Packer, and R.E. Kalina (1987a) A whole mount method for sequential analysis of photoreceptors and ganglion cells in a single retina. *Vision Res.* 27:9-15.
- Curcio, C.A., and K.R. Sloan Jr. (1986) Computer-assisted morphometry using video-mixed microscopic images and computer graphics. *Anat. Rec.* 214:329-337.
- Curcio, C.A., K.R. Sloan Jr., A.E. Hendrickson, and R.E. Kalina (1986a) Human photoreceptor topography as revealed by computer reconstruction and display of retinal whole mounts. *Invest. Ophthalmol. Vis. Sci.* 27[Suppl]:330.
- Curcio, C.A., K.R. Sloan Jr., A.E. Hendrickson, and R.E. Kalina (1986b) Individual variability in the topography of human photoreceptors. *Soc. Neurosci. Abstr.* 12:636.
- Curcio, C.A., K.R. Sloan, and D. Meyer (1989) Computer method for sampling, reconstruction, display and analysis of retinal whole mounts. *Vision Res.* 19:529-540.
- Curcio, C.A., K.R. Sloan Jr., O. Packer, A.E. Hendrickson, and R.E. Kalina (1987b) Distribution of cones in human and monkey retina: individual variability and radial asymmetry. *Science* 236:579-582.
- de Monasterio, F.M., E.P. McCrane, J.K. Newlander, and S.J. Schein (1985) Density profile of blue-sensitive cones along the horizontal meridian of macaque retina. *Invest. Ophthalmol. Vis. Sci.* 26:289-302.
- Drasdo, N., and C.W. Fowler (1974) Non-linear projection of the retinal image in a wide-angle schematic eye. *Br. J. Ophthalmol.* 58:709-714.
- Ederer, F. (1973) Shall we count number of eyes or number of subjects? *Arch. Ophthalmol.* 89:1-2.
- Farber, D.B., J.G. Flannery, R.N. Lolley, and D. Bok (1985) Distribution patterns of photoreceptors, proteins and cyclic nucleotides in the human retina. *Invest. Ophthalmol. Vis. Sci.* 26:1558-1568.
- Fine, B.S., and M. Yanoff (1972) *Ocular Histology*. New York: Harper & Row.
- French, A.S., A.W. Snyder, and D.G. Stavenga (1977) Image degradation by an irregular retinal mosaic. *Biol. Cybernet.* 27:229-233.
- Frisen, L. (1970) The cartographic deformations of the visual field. *Ophthalmology* 161:38-54.
- Fritsch, G. (1908) *Über Bau und Bedeutung der area centralis des Menschen*. Berlin: Reiner.
- Gartner, S., and P. Henkind (1981) Aging and Degeneration of the human macula. I. Outer nuclear layer and photoreceptors. *Br. J. Ophthalmol.* 65:23-28.
- Geisler, W.S., and D.B. Hamilton (1986) Sampling-theory analysis of spatial vision. *J. Opt. Soc. Am. A* 3:62-70.
- Green, D.G. (1970) Regional variations in the visual acuity for interference fringes on the retina. *J. Physiol. (Lond.)* 207:351-356.
- Groll, S.L., and J. Hirsch (1987) Two-dot vernier discrimination within 2.0 degrees of the foveal center. *J. Opt. Soc. Am. A* 4:1535-1542.
- Hartridge, H. (1950) *Recent Advances in the Physiology of Vision*. Philadelphia: Blakiston.
- Hawken, M.J., V.H. Perry, and A.J. Parker (1988) Structural relationships of photoreceptors to V1 receptive fields in the primate. *Invest. Ophthalmol. Vis. Sci.* 29[Suppl]:297.
- Helmholtz, H. (1924) *Treatise on Physiological Optics*, Vol. 2, The Sensation of Vision, transl. J.P.C. Southall, Optical Society of America.
- Hendrickson, A.E., and C. Yuodelis (1984) The morphological development of the human fovea. *Ophthalmology* 91:603-612.
- Hirsch, J., and C.A. Curcio (1989) The spatial resolution capacity of the human fovea. *Vision Res.* 29:1095-1101.
- Hirsch, J., and R. Hylton (1982) Limits of spatial frequency discrimination as evidence of neural interpolation. *J. Opt. Soc. Am.* 72:1367-1374.
- Hirsch, J., and R. Hylton (1984a) Orientation dependence of hyperacuity contains components with hexagonal symmetry. *J. Opt. Soc. Am. A* 1:300-308.
- Hirsch, J., and R. Hylton (1984b) Quality of the primate photoreceptor lattice and limits of spatial vision. *Vision Res.* 24:347-355.
- Hirsch, J., and W.H. Miller (1987) Does cone positional disorder limit resolution? *J. Opt. Soc. Am. A* 4:1481-1492.
- Hogan, M.J., J.A. Alvarado, and J.E. Weddell (1971) *Histology of the Human Eye*. Philadelphia: W.B. Saunders.
- Holden, A.L., B.P. Hayes, and F.W. Fitzke (1987) Retinal magnification factor at the ora terminalis: A structural study of human and animal eyes. *Vision Res.* 27:1229-1235.
- Latié, A., P. Liebmam, and C. Campbell (1968) Photoreceptor orientation in the primate eye. *Nature* 218:172-173.
- Ludvigh, E. (1941) Extrafoveal visual acuity as measured with Snellen test letters. *Am. J. Ophthalmol.* 24:303-310.
- Miller, W.H. (1979) Ocular optical filtering. In H. Autrum (ed): *Handbook of Sensory Physiology*. Berlin: Springer-Verlag. Vol VII/6A, pp. 70-143.
- Miller, W.H., and G. Bernard (1983) Averaging over the fovea receptor aperture curtails aliasing. *Vision Res.* 23:1365-1369.
- O'Brien, B. (1951) Vision and resolution in the central retina. *J. Opt. Soc. Am.* 1:882-894.
- Österberg, G.A. (1935) Topography of the layer of rods and cones in the human retina. *Acta Ophthalmol.* 13[Suppl 6]:1-97.
- Packer, O., A.E. Hendrickson, and C.A. Curcio (1988) Development of rod topography in pigtail macaque retina. *Invest. Ophthalmol. Vis. Sci.* 29[Suppl]:377.
- Packer, O., A.E. Hendrickson, and C.A. Curcio (1989) Photoreceptor topography of the adult pigtail macaque (*Macaca nemestrina*) retina. *J. Comp. Neurol.* 288:165-183.
- Perry, V.H., and A. Cowey (1985) The ganglion cell and cone distributions in

- the monkey's retina: Implications for central magnification factors. *Vision Res.* 25:1795–1810.
- Pirenne, M.H. (1967) *Vision and the Eye*. London: Associated Book Publ.
- Polyak, S.L. (1941) *The Retina*. Chicago: University of Chicago.
- Polyak, S.L. (1957) *The Vertebrate Visual System*. Chicago: University of Chicago.
- Pulos, E., and G. Bresnick (1988) Changes in rod sensitivity through adulthood. *Invest. Ophthalmol. Vis. Sci.* 29[Suppl]:446.
- Reymond, L. (1985) Spatial visual acuity of the eagle *Aquila audax*: A behavioral, optical and anatomical investigation. *Vision Res.* 25:1477–1491.
- Reymond, L. (1987) Spatial visual acuity of the falcon, *Falco berigora*: A behavioral, optical and anatomical investigation. *Vision Res.* 27:1859–1874.
- Rodieck, R.W. (1988) The Primate Retina. In H.D. Steklis and J. Erwin (eds): *Comparative Primate Biology*, New York: Alan R. Liss, Inc., pp. 203–278.
- Rolls, E.T., and A. Cowey (1970) Topography of the retina and striate cortex and its relationship to visual acuity in rhesus monkeys and squirrel monkeys. *Exp. Brain Res.* 10:298–310.
- Schein, S.J. (1988) Anatomy of macaque fovea and spatial densities of neurons in foveal representation. *J. Comp. Neurol.* 269:479–505.
- Schultze, M. (1866) Zur Anatomie und Physiologie der Retina. *Arch. Mikrosk. Anat.* 2:165–286.
- Sloan, L. (1968) The photopic acuity-luminance function with special reference to parafoveal vision. *Vision Res.* 8:901–911.
- Smith, R.A., and P.F. Cass (1987) Aliasing in the parafovea with incoherent light. *J. Opt. Soc. Am. A.* 4:1530–1534.
- Snyder, A.W., T.R.J. Bossomaier, and A. Hughes (1986) Optical image quality and the cone mosaic. *Science* 231:499–500.
- Snyder, A.W., and W.H. Miller (1977) Photoreceptor diameter and spacing for highest resolving power. *J. Opt. Soc. Am.* 67:696–698.
- Tessier-Lavigne, M., and D. Attwell (1988) The effect of photoreceptor coupling and synapse nonlinearity on signal: noise ratio in early visual processing. *Proc. R. Soc. London [Biol.]* 234:171–197.
- Thibos, L.N., F.E. Cheney, and D.J. Walsh (1987) Retinal limits to the detection and resolution of gratings. *J. Opt. Soc. Am. A.* 4:1524–1529.
- Tyler, C. (1985) Analysis of human receptor density. *Invest. Ophthalmol. Vis. Sci.* 26[Suppl]:10.
- Weiskrantz, L., and A. Cowey (1963) Striate cortex lesions and visual acuity of the rhesus monkey. *J. Comp. Physiol. Psychol.* 56:225–231.
- Wertheim, T. (1980) Peripheral visual acuity. Translated by I. Dunsky, *Am. J. Optom.* 57:915–924.
- Westheimer, G. (1982) The spatial grain of the perifoveal visual field. *Vis. Res.* 22:157–162.
- Weymouth, R., D. Hines, L. Acres, J. Raaf, and M. Wheeler (1928) Visual acuity within the area centralis and its relation to eye movements and fixation. *Am. J. Ophthalmol.* 11:947–961.
- Wikler, K.C., R.W. Williams, and P. Rakic (1988) Number, distribution and ratios of rods and cones in the adult macaque retina. *Soc. Neurosci. Abstr.* 14:1119.
- Williams, D.R., and R. Collier (1983) Consequences of spatial sampling by a human photoreceptor mosaic. *Science* 227:385–387.
- Williams, D.R. (1985) Aliasing in human foveal vision. *Vision Res.* 25:195–205.
- Williams, D.R. (1986) Seeing through the photoreceptor mosaic. *Trends Neurosci.* 9:193–198.
- Williams, D.R. (1988) Topography of the foveal cone mosaic in the living human eye. *Vision Res.* 28:433–454.
- Williams, D.R., and N.J. Coletta (1987) On defining the visual resolution limit. *J. Opt. Soc. Am. A.* 4:1514–1522.
- Yanoff, M., and B.S. Fine (1982) *Ocular Pathology*. Philadelphia: Harper & Row.
- Yellott, J.I. Jr. (1982) Spectral analysis of spatial sampling by photoreceptor topological disorder prevents aliasing. *Vision Res.* 22:1205–1210.
- Yuodelis, C., and A. Hendrickson (1986) A qualitative and quantitative analysis of the human fovea during development. *Vision Res.* 26:847–856.